Biomaterials 276 (2021) 121052

Contents lists available at ScienceDirect

Biomaterials

journal homepage: www.elsevier.com/locate/biomaterials

A rationally designed self-immolative linker enhances the synergism between a polymer-rock inhibitor conjugate and neural progenitor cells in the treatment of spinal cord injury

E. Giraldo [a,b], V.J. Nebot [c,d], S. Đorđević [c], R. Requejo-Aguilar [a,e], A. Alastrue-Agudo [a], O. Zagorodko [c], A. Armiñan [c], B. Martinez-Rojas [a], M.J. Vicent [c,*], V. Moreno-Manzano [a,**]

[a] Neuronal and Tissue Regeneration Lab. Prince Felipe Research Institute, Valencia, Spain
[b] Department of Biotechnology. Universitat Politècnica de València, Valencia, Spain
[c] Polymer Therapeutics Lab. Prince Felipe Research Institute, Valencia, Spain
[d] PTS S.L., Valencia, Spain
[e] Dept. Biochemistry and Molecular Biology, University of Cordoba, Cordoba, Spain. Maimonides Biomedical Research Institute of Córdoba (IMIBIC), Cordoba, Spain

ARTICLE INFO

Keywords:
Polymer therapeutics
Polymer-drug conjugates
Fasudil
Spinal cord injury
Axonal elongation
Neuroprotection
RhoA/ROCK Inhibitor

ABSTRACT

Rho/ROCK signaling induced after spinal cord injury (SCI) contributes to secondary damage by promoting apoptosis, inflammation, and axon growth inhibition. The specific Rho-kinase inhibitor fasudil can contribute to functional regeneration after SCI, although inherent low stability has hampered its use. To improve the therapeutic potential of fasudil, we now describe a family of rationally-designed bioresponsive polymer-fasudil conjugates based on an understanding of the conditions after SCI, such as low pH, enhanced expression of specific proteases, and a reductive environment. Fasudil conjugated to poly-L-glutamate via a self-immolative redox-sensitive linker (PGA-SS-F) displays optimal release kinetics and, consequently, treatment with PGA-SS-F significantly induces neurite elongation and axon growth in dorsal root ganglia explants, spinal cord organotypic cultures, and neural precursor cells (NPCs). The intrathecal administration of PGA-SS-F after SCI in a rat model prevents early apoptosis and induces the expression of axonal growth- and neuroplasticity-associated markers to a higher extent than the free form of fasudil. Moreover, a combination treatment comprising the acute transplantation of NPCs pre-treated with PGA-SS-F leads to enhanced cell engraftment and reduced cyst formation after SCI. In chronic SCI, combinatory treatment increases the preservation of neuronal fibers. Overall, this synergistic combinatorial strategy may represent a potentially efficient clinical approach to SCI treatment.

1. Introduction

The efficient treatment of spinal cord injury (SCI) remains challenging due to the dynamic and progressive nature of the condition conferred by the intrinsic pathological cascades involved. The implementation of complementary neuroprotective and neuroregenerative interventions represents one potential strategy to limit/rescue the neurological deficits induced by the secondary injury phase (previously reviewed by Ahuja and Fehlings [1]). The secondary injury phase involves the necrosis and/or apoptosis of neurons and glia, such as oligodendrocytes, thereby prompting demyelination and a loss of efficient neuronal connectivity. Furthermore, the induction of an ischemic environment leads to ongoing edema, vessel thrombosis, and vasospasms, while persistent inflammatory cell infiltration causes the continuing formation of toxic cystic microcavities. Astrocytes, fibroblasts, and pericytes proliferate and deposit extracellular matrix factors into the perilesional area in the intermediate and chronic phases when damaged axons continue to degenerate (previously reviewed by Bradbury and Burnside [2]). Overall, studies attribute both microenvironmental extrinsic factors and a limited intrinsic axon regrow capacity to the lack of spontaneous regeneration observed during and after chronic stage injury.

RhoA/ROCK activation represents a major intrinsic inhibitory signal for axonal regrowth [3] by promoting apoptosis, growth cone collapse in

* Corresponding authors.
** Corresponding authors.
E-mail addresses: mjvicent@cipf.es (M.J. Vicent), vmorenom@cipf.es (V. Moreno-Manzano).

https://doi.org/10.1016/j.biomaterials.2021.121052
Received 29 January 2021; Received in revised form 4 July 2021; Accepted 24 July 2021
Available online 29 July 2021
0142-9612/© 2021 The Authors. Published by Elsevier Ltd. This is an open access article under the CC BY-NC-ND license (http://creativecommons.org/licenses/by-nc-nd/4.0/).

regenerating axons, and subsequent neurite retraction [4]. For these reasons, RhoA/ROCK activation also represents a critical therapeutic target [5]. The RhoA/ROCK inhibitor fasudil (1-(5-isoquinolinesulfonyl)-homopiperazine) can suppress secondary damage by reducing edema, inflammatory cell infiltration, cyst cavitation, and massive apoptosis in acute stage SCI [6]. While the application of fasudil in the treatment of subarachnoid hemorrhage has provided evidence of safety, fasudil displays limited clinical efficacy [7], perhaps due to a short half-life and, of significant note for SCI treatment, a lack of penetration through the blood-brain barrier [8]. These problems, alongside the requirement to improve the site-specific activity and bioavailability, have prompted the exploration of nanocarrier formulations as a potential solution, with the vast majority taking advantage of drug encapsulation [9]. Studies have also provided evidence for the utility of rationally designed polymer-drug conjugates [10,11] as novel therapeutics for SCI using neuroprotectants such as curcumin [12].

Polypeptide-based polymers, particularly poly-L-glutamic acid (PGA), are biocompatible, biodegradable, and multifunctional nanocarriers that allow for high drug loading capacity [13,14]. Polypeptides have been employed as building blocks in the development of polymer-drug conjugates and polymeric micelles for various medical applications [13]. The routine clinical use of Copaxone® [13,14] and the promising clinical results observed with polypeptidic micelles [15] and Opaxio® [13,14,16] have underscored the potential of synthetic polypeptides. Conjugated active agents can be released from PGA thanks to the activity of proteases such as lysosomal protease cathepsin B [17] after engineering polymer side chains [18]. Furthermore, post-polymerization modification reactions provide orthogonal reactive attachment sites for a variety of functionalities for further bioconjugation [19], thereby allowing the conjugation of drugs through rationally-designed bioresponsive linkers that can modify drug release kinetics at sites of injury, such as SCI. Said linkers include those that display pH-responsiveness [12,20] or redox-sensitivity [13,14]. Additional aspects of PGAs that support their application in SCI treatment include an inherently negative z-potential that facilitates the targeting of inflamed areas [21]. Of note, synthetic challenges related to the tight control of PGA properties have been overcome through the development of precise and controlled reactions and characterization steps to yield well-defined polypeptidic architectures [22–24].

In addition to the formation of a permissive platform bridging the extrinsic inhibitory microenvironment in SCI, cell transplantation also affords neuroprotection and prompts immunomodulation [1]. The transplantation of fetal neural progenitor cells (NPCs) [25,26] and induced pluripotent stem cells (iPSCs) [27] have provided promising results in terms of repair and neuronal regeneration [28]. Interestingly, regenerating endogenous axons navigate through NPC grafts to their appropriated sensory and motor targets, indicating that cell transplantation can correctly guide re-innervation without additional exogenous signals [29]. NPCs include multipotent stem cells present in the ependymal region lining the spinal cord's central canal [30], which represent ideal candidates for stem cell therapy due to the functional improvements observed after transplantation and the absence of malignant transformation. We previously established that NPC transplantation in both acute [31–33] and chronic [12] traumatic SCI led to the rescue of voluntary locomotion after one week. Contributing mechanisms induced by NPC transplantation include trophic support, immunomodulation, and the reduction of inhibitory mediators, such as the purinergic receptors associated with neurodegenerative and neuropathic pain. Overall, NPC transplantation can drive the formation of a microenvironment conducive to the preservation of neurons, a reduction in the number of cavities, and the inhibition of scar formation.

Even given these promising results, the limited functional and anatomical improvements obtained in rat models, with poor cell survival as a significant contributor, suggest that NPC transplantation alone will fail to provide sufficient gain of function to foster further clinical development. We have demonstrated that combining a rationally-designed bioresponsive polyacetal-curcumin conjugate with NPC transplantation significantly enhances therapeutic outcomes via an anti-inflammatory effect and axonal growth via the inhibition of RhoA/ROCK signaling [12]. Herein, we demonstrate that a combination of NPC transplantation and an improved nanoformulation of a Rho kinase inhibitor (fasudil) may represent an efficient alternative treatment for SCI. We developed and optimized a family of bioresponsive PGA-based fasudil conjugates and found that the best candidate, which employed a redox-triggered self-immolative linker, synergized with NPCs to trigger significant levels of axonal regrowth in organotypic cultures, enhanced cell engraftment and a certain locomotor skill recovery in an SCI model after acute administration, and neuronal fiber preservation in a chronic SCI model.

2. Materials and methods

2.1. Synthesis of Poly-L-glutamate (PGA)-Fasudil conjugates

Experimental details for the synthesis of intermediate compounds and final conjugates and the physico-chemical characterization are detailed in the Supporting Information (1. Materials and Experimental Techniques; 2. Synthesis and Physico-chemical Characterization of PGA-X-F Conjugates).

2.2. Fasudil Release Kinetics from conjugates under physiological conditions

2.2.1. pH-dependent drug release kinetics

Specific fasudil release under mildly acidic conditions was demonstrated in vitro by incubating the conjugates at 2 mg/mL in phosphate-buffered saline (PBS) at pH 7.4 and pH 5.0, mimicking the blood and tumor (and/or lysosomal) environment, respectively. At determined time points, 100 μL aliquots were made up to 1 mL with phosphate buffer (PB) pH 7.4 in a 15 mL tube. Liquid-liquid extraction of released fasudil and its quantification by reversed-phase high-performance liquid chromatography (RP-HPLC) was performed employing a Waters instrument equipped with an autosampler (Waters 717), two binary pumps, and a photodiode array detector (Waters 2996). Detection was carried out at $\lambda = 323$ nm (peak characteristic of the drug, mobile phase: H_2O (1 % NH_3)/MeOH (40/60), at a retention time of 6 min) using a column InertSustain C18, 5 μm, 4.6 × 250 mm modified with octadecylsilyl groups. The injection volume was 20 μL, while the flow rate of the mobile phase was set at 1.0 mL/min. The calibration curve was generated using fasudil, showing a linear response within the concentration range employed (1.5–20 μg/mL).

2.2.2. Cathepsin B-dependent drug release kinetics

Cathepsin B (5 U) was added to a solution of 2 mg of each conjugate in 1 mL of a pH 6 buffer composed of 20 mM sodium acetate, 2 mM ethylenediaminetetraacetic acid (EDTA), and 5 mM dithiothreitol (DTT). The incubation was carried out at 37 °C. Aliquots (100 μL) were taken at times up to 72 h, immediately frozen in liquid nitrogen, and stored in the absence of light until assayed by HPLC, as described above. The free drug (0.2 mg/mL) was also incubated under the same conditions and later used as the reference control to determine the percentage of release, as was a control solution without cathepsin B.

2.2.3. Redox-dependent drug release kinetics

DTT (100 μL of 50 mM or 100 μM solution in PBS) was added to a solution of 2 mg of PGA-SS-F (the equivalent of 0.236 mg/mL of fasudil) in 0.9 mL PBS to obtain a final DTT concentration of 5 mM or 100 μM. The incubation was carried out at 37 °C. Aliquots (100 μL) were taken at times up to 72 h and assayed by HPLC, as described above.

2.3. Stability of PGA-SS-F in plasma and cell medium

The stability studies of the PGA-SS-F conjugate was carried out by spiking blank human plasma and cell medium with the appropriate working solutions to achieve concentrations of 400 μg/mL PGA-SS-F and 1 ng/mL ranitidine as an internal standard (IS). Plasma samples were incubated at 37 °C and aliquots taken at 0, 2, 4, 6, and 24 h. Subsequently, 250 μL of acetonitrile was added to 100 μL of collected plasma and cell medium aliquots, followed by vortex-mixing for 30 s and centrifugation at 11,000 rpm for 5 min. Supernatants were then carefully removed, transferred to new tubes, and evaporated under nitrogen. The residue was reconstituted in 100 μL of the mobile phase, followed by vortex-mixing for 1 min. Finally, 20 μL of each solution was injected for liquid chromatography-mass spectrometry (LC-MS/MS) analysis.

2.3.1. LC-MS/MS method for determination of fasudil in plasma and cell medium

Chromatographic analysis was performed using an ExionLC system comprising of a Pump, AC Autosampler, AC Column oven, and AB Sciex QTRAP 4500 (all Sciex, Singapore). The initial mobile phase composition was acetonitrile:formic acid (0.1%) (20:80, v/v). All runs were performed using a Phenomenex Luna®-C18 column (4.6 mm × 30 mm, 5 μm), which was maintained at 40 °C. The injection volume was 10 μL, while the flow rate of the mobile phase was set at 0.4 mL/min. Fasudil and ranitidine as IS were detected in positive electrospray mode, with multiple reactions monitoring scan and by following two mass transitions 292.4 m/z → 99.2 m/z and 292.4 → 129.0 m/z for fasudil, and 315.2 m/z → 101.9 m/z and 315.2 m/z → 130.0 m/z for ranitidine. The LC-MS/MS method was developed using an experimental design approach, where the percentage of acetonitrile, percentage of formic acid, and flow rate from LC conditions and five factors from MS (ion spray voltage (3000–5500 V), the temperature of ion source (300–750 °C), curtain gas pressure (20–40 psi), nebulizer (Gas 1) gas pressure (20–60 psi) and auxiliary (Gas 2) gas pressure (40–80 psi)) were selected as factors that may have a significant effect on ionization efficiency. The influence of collision energy (CE), collision cell exit potential (CXP), entrance potential (EP), and declustering potential (DP) on the fasudil peak area was evaluated using a "One Factor at A Time" approach, as these parameters do not interact with each other. Design of experimental plans and data analysis in the experimental design approach were performed with Design-Expert® 11.0.0 software (Stat–Ease Inc., USA), while data acquisition employed Analyst® software (AB Sciex, Singapore).

Validation of the developed LC-MS method was carried out according to "Guideline on bioanalytical method validation, (July 21, 2011 EMEA/CHMP/EWP/192217/2009 Rev. 1 Corr. 2, Committee for Medicinal Products for Human Use (CHMP))" from the European Medicines Agency. The validation parameters evaluated were linearity, the limit of quantification (LOQ), limit of detection (LOD), recovery, accuracy, precision, stability, and matrix effects. A stock solution (1 mg/mL) and working solutions (10 μg/mL) of fasudil hydrochloride and ranitidine hydrochloride were assessed for storage stability for 48h at −20 °C. Stock solutions were diluted from 1 mg/mL to 10 μg/mL and analyzed together with 10 μg/mL working solutions of fasudil and ranitidine. Linearity was evaluated by constructing a calibration curve obtained by the internal standard method, where fasudil and ranitidine peak area ratios were plotted vs. fasudil and ranitidine concentration ratio. Eight concentrations were used for constructing the calibration curve for fasudil (10, 20, 50, 100, 200, 400, 800, and 1000 ng/mL) with the addition of ranitidine in the concentration of 1 ng/mL. LOD and LOQ values were calculated from the LINEST function, while precision and accuracy were evaluated in two manners - within-run precision/accuracy and between-run precision/accuracy. Three plasma samples were spiked with fasudil and ranitidine at low-quality control level (LLOQ- 10 ng/mL), medium quality control level (medium QC- 500 ng/mL), and upper-quality control level (ULOQ- 1000 ng/mL) and analyzed in a single run for testing within-run precision/accuracy, while four runs on two different days were performed for between-run precision/accuracy. Matrix effects were tested with two different sample types i) blank plasma/cell medium spiked after sample preparation with fasudil at LLOQ, medium QC, and ULOQ level, and with 1 ng/mL of ranitidine and ii) water solution of fasudil and ranitidine in the same concentration as spiked samples (LLOQ, medium QC and ULOQ level for fasudil and 1 ng/mL for ranitidine). Recovery was assessed on three QC levels by comparing the mass of extracted analyte and analyte in the sample (plasma/cell medium spiked after the sample preparation) and represented as a percentage.

2.4. LC-MS method for the determination of total fasudil content in cerebrospinal fluid

2.4.1. Sample preparation

50 mM DTT was added to 20 μL of cerebrospinal fluid (CSF) samples (collected 48 h after administration of PGA-SS-F [300 μM fasudil equiv.] to animals) to induce the total release of fasudil from the PGA-SS-F conjugate. Then, 50 μL of acetonitrile was added to the sample for protein precipitation, vortex-mixed for 30 s, and centrifuged at 11,000 rpm for 5 min. The supernatant was carefully removed, transferred to fresh tubes, and dried by evaporation. The residue was reconstituted in 20 μL of acetonitrile followed by vortex-mixing for 1 min, and finally, 10 μL of the solution was injected for LC-MS analysis.

2.4.2. LC-MS/MS method for the determination of fasudil in the CSF

The LC-MS/MS conditions employed were identical to those used above for the analysis of fasudil stability in plasma. Nevertheless, the developed LC-MS and extraction methods were re-evaluated for linearity, LOQ, LOD, recovery, and matrix effects. Linearity was evaluated by constructing a calibration curve obtained by the internal standard method, where fasudil and IS peak area ratios were plotted vs. fasudil and IS concentration ratio. Six concentrations were used to construct the calibration curve for fasudil (up to 250 ng/mL) with the addition of ranitidine at a concentration of 2.5 ng/mL. LOD and LOQ values were calculated from the LINEST function. Recovery was assessed by comparing the mass of extracted analyte and analyte in the CSF spiked after the sample preparation, presented as a percentage. Matrix effects were evaluated by comparing two samples - one sample with blank CSF spiked after sample preparation with fasudil at ULOQ (250 ng/mL) and with 2.5 ng/mL of ranitidine, and another sample of a water solution of fasudil and ranitidine in the same concentration as spiked samples.

2.5. NPC isolation, cell culture, and experimental conditions

NPCs or eGFP-NPCs [32] were harvested from neonatal (P4-6) Sprague Dawley-Tg (GFP) 2BalRrrc rats. eGFP+/+ homozygote rats were used for organocultures and cell transplantation for in vivo experiments, while eGFP−/− rats for all in vitro assays. Spinal cords were dissected after complete laminectomy, and the overlying meninges and blood vessels were removed. The dissected tissue was cut into 1 mm^3 segments and mechanically homogenized without enzymatic treatment. NPCs were isolated and cultured as neurosphere-like form in growth medium in low-attachment plates (DMEM/F12 supplemented with 100 U/mL penicillin, 100 μg/mL streptomycin, 2 mM L-glutamine, 5 mM HEPES buffer, 0.125% NaHCO3, 0.6% glucose, 0.025 mg/mL insulin, 80 μg/mL apotransferrin, 16 nM progesterone, 60 μM putrescine, 24 nM sodium selenite, 4 μg/mL BSA, 0.7 U/mL heparin, 20 ng/mL EGF and 20 ng/mL bFGF, 1 mM N-acetyl-cysteine (NAC)). For adherent conditions, NPCs were cultured on Matrigel® coated coverslips diluted 1/10 in growth medium. To assess spontaneous differentiation of NPCs, neurospheres were dissociated with Accutase following manufacturer instructions and then seeded onto Matrigel® coated coverslips in differentiation media (DMEM/F12 supplemented with 1 mM NAC, 100 U/mL penicillin, 100 μg/mL streptomycin, 2 mM L-glutamine, 5 mM

HEPES buffer, 0.125% NaHCO3, 0.6% glucose, 0.025 mg/mL insulin, 80 μg/mL apotransferrin, 16 nM progesterone, 60 μM putrescine, 24 nM sodium selenite, 2 % fetal bovine serum) for seven days. Pharmacological treatments (LPA, PGA-SS-F or F) were added at the day three of culture and maintain till cell fixation at day seven.

To determine the effect of fasudil or conjugates on proliferation, cell vibility, differentiation and neurite elongation, NPC cultures were treated with 50 or 100 μM of each compound for 24h, 48 h, and 72 h. Neurite length was evaluated using Incucyte NeuroTrack analysis software™ (Cat. 9600–0010) when performed in phase-contrast images (Fig. 3D and Figure SI8C) and using the NeuronJ plug-in from ImageJ in Nestin stained cultures (Fig. 6A,D and Figure SI9) as previously described [34]. In vitro neurite retraction was induced by adding 10 μM of LPA (L726, Sigma) to the cultures for 24 h after fasudil or PGA-SS-F treatments. For the exploration of the role of 5′ adenosine monophosphate-activated protein kinase (AMPK) activation in PGA-SS-F-induced neurite outgrowth, NPCs were treated with an AMPK inhibitor (10 μM Compound C; Merck CAS 866405-64-3) before LPA and/or fasudil or PGA-SS-F treatment (Figure SI10).

2.6. Cellular uptake studies

2.6.1. Live-cell confocal imaging

Uptake assays were performed in non-adherent NPC cultures at 37 °C and 4 °C. Cells were seeded in ultra-low attach six-well plates at 1 x 10^6 cells/cm^2 and incubated for 24 h. A cathepsin B inhibitor, leupeptin (PanReac AppliChem, VWR, U.E.), was added to each well at 10 μM 30 min before the incubation of conjugates (PGA-F-OG, PGA-O-F-OG, and PGA-SS-F-OG) to avoid degradation. To perform the 4 °C uptake experiment, cells were pre-incubated at 4 °C for 30 min before the addition of the treatments. 12 μg/mL of each polymer were evaluated at different time points (0–300 min). Cell medium was subsequently removed, cells were washed twice with PBS 0.1 wt% BSA (Bovine serum albumin, Sigma-Aldrich, Spain, UE), and then cells were collected in 500 μL of PBS 0.1 wt % BSA and transferred into confocal multiwell plates. Lysotracker-deep red (ThermoFisher) was added, and cells were incubated for 30 min. The percentage of OG-positive cells was evaluated for each treatment after confocal image acquisition in triplicate. Co-localization analysis in the confocal analysis was performed using lysosomes labeled with Dextran-TR (red) co-incubated from time zero in all tested conditions and replicates. Consistent exposures were applied for all images.

2.7. Dorsal root ganglia (DRG) explants and spinal cord (SC) organotypic cultures: experimental conditions, sample preparation, image acquisition, and analysis

DRG explants and SC slices were dissected from five-day-old Sprague-Dawley GFP-/- rats. DRG explants were placed on poly-L-lysine/laminin-coated coverslips and cultured for ten days in neurobasal medium, supplemented with B27, 1 mM N-acetyl cysteine (NAC), 2 mM GlutaMAX, 10 % fetal bovine serum, and 1 % penicillin/streptomycin. Two days after plating DRGs, 50 μM of PGA-SS-F or fasudil were added to the culture media, and the explants were incubated for eight additional days. After fixation, the whole DRG explant and surrounding outgrowth of axons were imaged using a sequential image mapping technique supported by Leica software, in which individual images were stitched together for final analysis. Axonal outgrowth from DRG explants was quantified by beta-III-tubulin staining and the NeuriteJ plug-in from ImageJ as previously described [34]. For GAP43 quantification, iamges were thresholded and positive area for GAP43 was quantified. Analyses were performed for seven DRG explants from four different experiments.

SC slices were cleaned out from meningeal layers and cut with a McIlwain Tissue Chopper in 350 μm thick slices in the transverse and parasagittal longitudinal plane. Immediately after, the slices were transferred onto Millicell-CM® (Millipore) inserts and placed into six-well plates with 1 mL of culture medium (50 % Minimum Essential Medium, 25 % Hanks' Balanced Salt Solution, 25 % horse serum, 2 mM GlutaMAX, 1 mM NAC, 0.5 % $NaHCO_3$ and 1 % penicillin/streptomycin). To generate a gap of damaged and spared axons, mimicking an ex vivo model of SCI, a complete transverse section with a scalpel blade was performed on cultures after five days in vitro, as described previously [35]. After transection, slices were treated with 50 μM fasudil or PGA-SS-F and cultured for seven more days. Then, tissues were fixed with 4 % paraformaldehyde for immunohistochemical analysis (three different slices for at least three animals were used per experimental condition). Consistent exposures were applied for all images. Quantitative analysis of neurofilaments and synaptophysin and PSA-NCAM levels was conducted by quantifying positive area on the maximal intensity projection images from five images per slice.

2.8. Immunocytochemistry

Paraformaldehyde-fixed cells and organotypic cultures were permeabilized with 0.1% Triton X-100 and subsequently blocked with 5% normal goat serum in PBS. The primary antibodies were incubated overnight at 4 °C: nestin (1:500 ab6142, Abcam), anti-beta-III-tubulin (1:500 MO15013, Neuromics), anti-GAP43 (1:500 ab128005, Abcam), synaptophysin (1:400 sc-17750, Santa Cruz), anti-GFP (Abcam), anti-Olig2 (1:500 ab33427, Millipore), anti-MAP2 (1:1000 AB3096, Abcam), anti-GFAP (1:1000 PA1-10004, ThermoFisher), Ki67 (1:500 ab15580, Abcam), and caspase-3 (1:500 9662S, Cell Signaling). After washing, secondary antibodies (anti-mouse, 1:5000 SC-516102, Santa Cruz, or anti-rabbit, 1:5000 SC-2357, Santa Cruz) were incubated for 2 h at R.T. The Phalloidin probe conjugated with Alexafluor647 was used at 1:1000 dilution (P1951 Sigma-Aldrich). All cells were counterstained by incubation with 4,6-diamidino-2-phenylindole dihydrochloride (DAPI; Invitrogen). Apotome Zeiss microscope was used for image acquisition of cell cultures. Confocal microscope SP8 (Leica) was used for image acquisition of DRG explants and organotypic cultures.

2.9. Western blot analysis

Total protein was extracted from spinal cord tissues or cell cultures using a lysis buffer containing 50 mM Tris-HCl, pH 7.5, 150 mM NaCl, 0.02% NaN3, 0.1% SDS, 1% NP40, 1 mM EDTA, 2 mg/mL leupeptin, 2 mg/mL aprotinin, 1 mM PMSF, and 1 x Protease Inhibitor Cocktail (Roche Diagnostics, San Diego, CA, USA). The protein concentrations of the supernatant were determined using the bicinchoninic acid (BCA) Protein Assay Kit (Thermofisher Scientific) and stored at −80C. An equal number of proteins (30 μg/well) were separated (10 % SDS-PAGE) and transferred to a polyvinylidene fluoride (PVDF) membrane. The membrane was blocked with 1 % BSA in Tris buffer saline (TBS) with 0.1 % Tween-20 for 1 h at room temperature and incubated at 4 °C overnight with the following primary antibody solutions: pAKT (1:1000 4060, Cell Signaling), Bag-1 (1:1000 sc-376848, Santa Cruz), Bcl-2 (1:1000 2870S, Cell Signaling), BDNF (1:500 sc-655114, Santa Cruz), cAMP (1:500 ab24851, Abcam), caspase-3 (1:1000 9662S Cell Signaling), p-MYPT (1:1000 ABS45 Millipore), and p-mTOR (1:1000 2971 Cell Signaling).; AMPK (1:1000 2535 Cell Signaling), LC3I (1:1000 3868 Cell Signaling). To ensure loading with equal amounts of protein lysates, blots were incubated with an antibody against β-tubulin (1:10,000 SIGMA) as a loading control. Signal detection was performed with an enhanced chemiluminescence kit (ECL Plus Western blotting detection reagent - G. E. Healthcare, Piscataway Township, NJ, USA), and bands were developed using Amersham Imager 600. The relative protein expression was quantified by Image Studio Lite software.

2.10. Animals, spinal cord contusion model, and treatments

Female Sprague Dawley rats (~200 g) were bred at the Animal

Experimentation Unit of the Research Institute Príncipe Felipe (Valencia, Spain). The maintenance and use of all animals were in accordance with the National Guide for the Care and Use of Experimental Animals Committee (Animal Care Committee of the Research Institute Principe Felipe) (Real Decreto 1201/2005). The rats were housed under standard temperature conditions with controlled 12 h light/dark cycles with ad libitum access to food and water. Severe SCI by contusion at thoracic segment T8 was performed applying 250 kdyn using Infinite Horizon Impactor, as previously described [36]. The experimental groups and the details of the number of animals included for each analysis for acute and chronic SCI models are indicated in Table S1. eGFP-NPCs aliquots for grafting were prepared immediately before injection at a density of 100,000 cells/μl. 10 μL of an eGFP-NPC suspension were intramedullary transplanted for distribution in rostral and caudal regions at a distance of 2 mm from the lesion at a rate of 2 μl/min using a siliconized pulled glass pipette. In the acute SCI model, PGA-SS-F-pretreated eGFP-NPCs were transplanted immediately after contusion. In the chronic SCI model, the eGPF-NPC and sustained compound delivery were applied five weeks after the SCI.

Intrathecal drug delivery was performed using a catheter introduced immediately below the thoracic injured segment, as previously described [36]. For administration of the compounds, 10 μL of PGA, PGA-SS-F, or free fasudil to reach a final concentration of 300 μM in the CSF was delivered throught the catheter. Animals were sacrificed 48 h after SCI and treatments, and CSF and spinal cord tissue were collected for further analysis. For sustained intrathecal drug delivery in the chronic SCI model, the catheter was connected to an osmotic pump Model 1007D filled with 100 μL of 10 mM solution of each of the compounds (PGA, or PGA-SS-F or fasudil) to deliver 1 μL/h of for seven days. After one week, the catheter and the pump were removed. Two months after treatment, all animals were sacrificed.

All animals were subjected to post-surgery care and passive and active rehabilitation protocols, as previously described [36]. Rats received subcutaneous injections of cyclosporin A (10 mg/kg) starting one day before transplantation and administered daily for one month. All animals were sacrificed two months after transplantation. Gait analysis was performed by the CatWalk® (Noldus, Asheville, NC, http://www.noldus.com) video-based system for automated gait analysis. Paw contact was quantified by counting high-intensity pixels as the mean of at least three rounds per analysis [37].

2.11. Histological analysis

Rats were overdosed via an intraperitoneal administration of sodium pentobarbital (100 mg/kg) and transcardially perfused with 0.9 % saline followed by 4% paraformaldehyde in PBS. Spinal cord tissue was cryopreserved with 30 % sucrose before inclusion in Tissue-Teck OCT (Sakura Finetek, U.S.A). Coronal (in acute SCI model) or longitudinal (in chronic SCI model) sections at the lesion epicenter were obtained with a cryostat set at 10 μm thickness. For the evaluation of cysts/cavities, every fifth collected section was stained with hematoxylin and eosin in an automatized station (Autostainer XL Leica) and scanned in an Aperio Versa scanner (Leica Biosystems). Images of approximately 12 mm length of the spinal cord (including the epicenter of the lesion) were analyzed with the Image Scope software. The total cyst/cavity area was normalized to the total analyzed spinal cord tissue. Immunofluorescence double staining following the previously detailed methodology was performed using beta-III-tubulin for neuronal fiber detection, GFAP for glial scar analysis, and Olig2 and NeuN for oligodendrocyte and neuron quantification, respectively. All samples were counterstained by incubation with DAPI. All quantified specific signals for each marker were normalized by the total analyzed area at equivalent tissue lengths, including the epicenter of the injury, in all groups using ImageJ software. The glial scar was measured via the lack of GFAP expression. The directionality analysis of beta-III-tubulin positive fibers analysis was performed using ImageJ/Fiji software and the Directionality plug-in.

2.12. Statistical analysis

Data presented as mean ± standard error of the mean (SEM) and analyzed using Graph Pad Prism Software. The Shapiro-Wilk normality test was performed to ensure normal data distribution. Comparisons between two groups and among multiple groups used unpaired Student's t-test and one-way ANOVA, using Tukey multiple comparison test for post-hoc analysis. If normality was not met, non-parametric tests were used - the Mann-Whitney rank-sum test and the Kruskal-Wallis One-way ANOVA with Dunn's method post hoc correction. P values ≤ 0.05 were considered statistically significant.

3. Results

3.1. Rational Design of PGA-Fasudil Conjugates and Polymer-drug Linker Optimization: Synthesis, Characterization, Stability, and Fasudil Release Kinetics in Physiological Media

To overcome the pharmacological limitations of fasudil (low half-life in plasma), we prepared a family of PGA-fasudil conjugates. Fasudil possesses only one accessible functional group - the secondary amine in the diazepane ring; therefore, our synthetic strategy aimed to introduce a range of bioresponsive polymer-drug linkers through this secondary amine to achieve optimized drug release kinetics and maximize the therapeutic value of fasudil with regards to SCI treatment.

We conjugated fasudil to PGA using three linkers with differing bioresponsiveness - PGA-F employs an amide linker degraded by proteolytic enzymes such as cathepsin B; PGA-O-F employs a hydrolytically-labile carbamate linker; and PGA-SS-F employs a self-immolative disulfide linker susceptible to reducing environments. As shown in Fig. 1A, we prepared the amide-linked conjugate by the direct conjugation of the secondary amide of fasudil to the carboxylic groups of PGA using DMTMM (4-(4,6-dimethoxy-1,3,5-triazin-2-yl)-4-methyl-morpholinium chloride) as a coupling agent [19]. We prepared the carbamate linked conjugate in two steps using a 2-propyn-2-ol carbamate derivative of fasudil conjugated to an azide-modified PGA using a click reaction (see details in Figure SI1). We prepared the self-immolative disulfide-linked conjugate in four steps, as shown in Figure SI1. The first step comprised the thiol exchange between pyridyl disulfide with mercaptoethanol, while the next two steps involved alcohol activation with *p*-nitrophenyl chloroformate and the consequent reaction with fasudil. The last step comprised the second thiol exchange with cysteamine hydrochloride and compound conjugation to PGA through DMTMM-mediated amide coupling. We observed general instability for product Fas-SS (IC4), with significant degradation after 48 h even at −80 °C; therefore, we performed the last coupling step immediately after compound preparation. Characterization of all intermediates demonstrated high purity and unequivocal assignments of identity (See Figure SI2).

We obtained the desired conjugates (Table 1) with high purity, yield, and conjugation efficiency (See full characterization in Fig. 1B–D and Figure SI3 and SI4). ^{1}H NMR experiments (Fig. 1B and Figure SI3) depict the typical broadening of the signals from the drug for all conjugates consistent with the conjugation of large molecular weight polymer and therefore reduced relaxation times. UV–Vis analysis allowed the determination of total drug loading, which was in a range of 11.5–13.7% (wt) (Figure SI3), while HPLC analysis established a free drug content of below 0.1 % wt of total drug loading in all three conjugates. Dynamic light scattering (DLS) analysis demonstrated that all conjugates possessed similar hydrodynamic radius values in PBS (close to 5 nm), which is consistent with unimeric polymer-drug conjugate entities (Fig. 1C and Figure SI4). Additionally, we found a z-potential of approximately −40 mV [13,38]. Size exclusion chromatography (SEC) analysis (Figure SI4) confirmed the homogeneous conjugation of fasudil throughout the polypeptide molecular weight distribution (by ultraviolet [UV] and refractive index [RI]).

Next, we studied the kinetics of fasudil release in conditions relevant

A

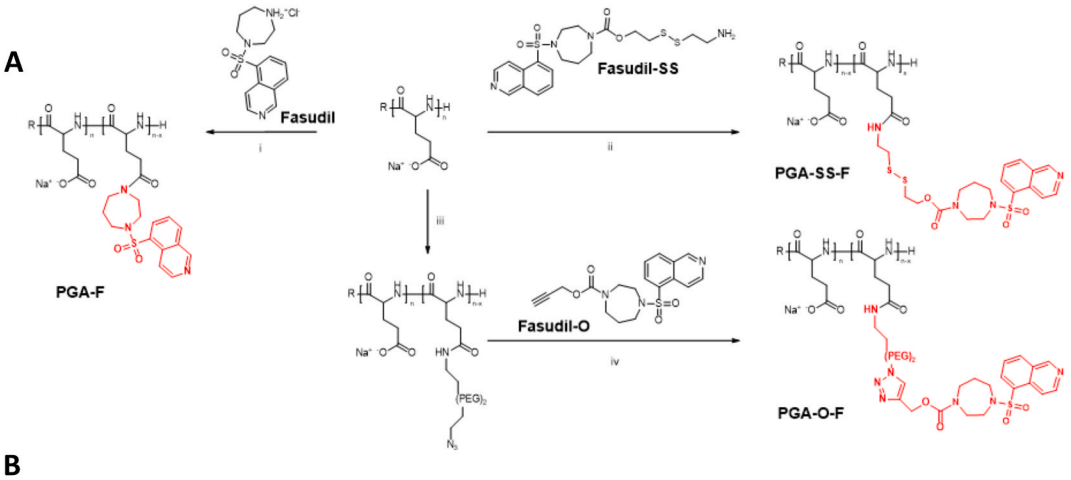

B

Conjugate	Linker	Yield, %	Conj. eff., %	TDL, %wt[a]	FD, %wt[b]	R_h, nm[c]
PGA-F	Amide	87	92	13.7	0.01	4,8
PGA-O-F	Carbamate	65	87	12.4	0.1	4,9
PGA-SS-F	Self-immolative disulfide	84	85	11.5	0.1	5,1

[a]Determined by UV-Vis. [b]Determined by HPLC (UV-Vis) and calculated as % of the total drug loading. [c]Hydrodynamic radius measured via DLS instrument in PBS expressed as mean Volume value.

C

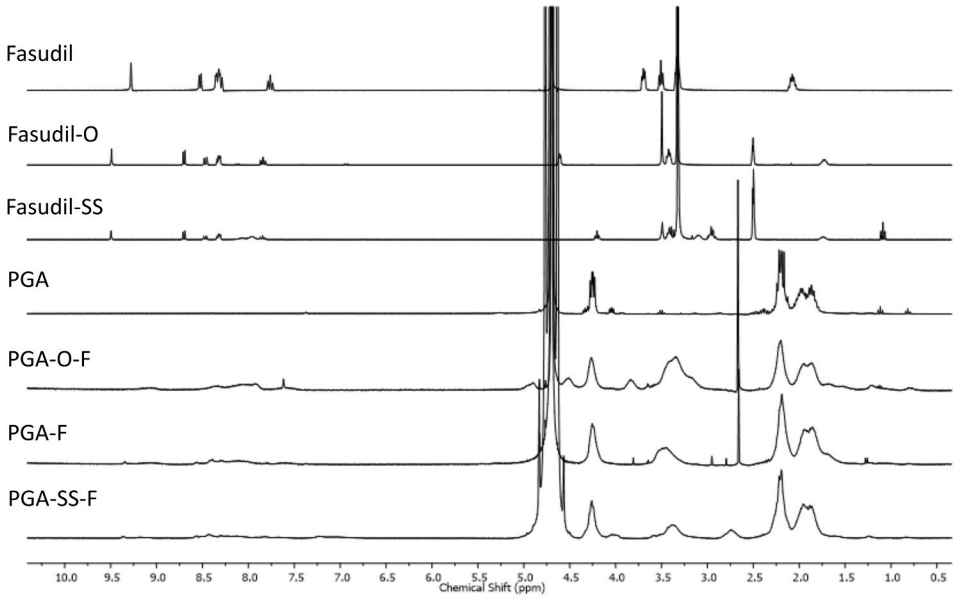

D

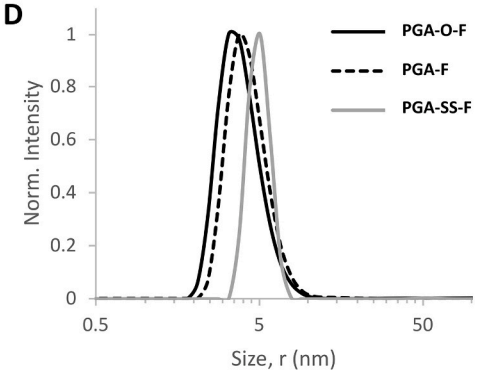

E

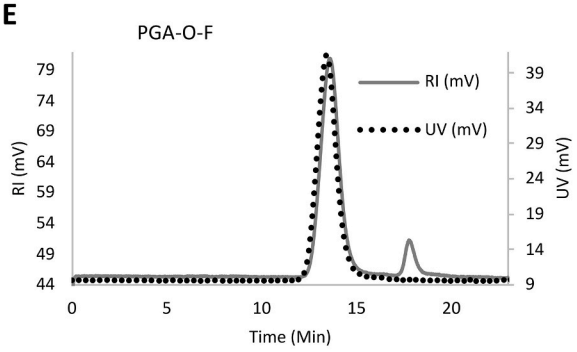

(caption on next page)

Fig. 1. Synthesis and Characterization of Polypeptide-based Fasudil Conjugates. A. Synthetic route for the preparation of the PGA-fasudil conjugate family. PGA-fasudil conjugates with amide (PGA-F), carbamate (PGA-O-F), self-immolative disulfide (PGA-SS-F) linking moieties were prepared according to the schematic. Reaction conditions were: i) H_2O, DMTMMCl, fasudil hydrochloride; ii) DMF, $DMTMMBF_4$, self-immolative disulfide fasudil-derivative; iii) H_2O, DMTMMCl, NH_2-$(CH_2)_2$-$(PEG)_2$-N_3 iv) DMF/H_2O, $CuSO_4$, sodium ascorbate, carbamate fasudil-derivative. B. Chemical identity and purity assessed via ^{1}H-NMR spectroscopy suggest the successful generation of the desired compounds. Upon conjugation to PGA, a broadening of the bands can be observed, although the characteristic peaks of the parent drug derivative are maintained; C. Size distribution (Rh, volume) of fasudil conjugates by DLS, 3 mg/mL in PBS. D. Size-exclusion chromatograms for all conjugates exhibit narrow molecular weight distribution (UV channel detected at 323 nm) throughout the polypeptide population (RI channel). The PGA-SS-F conjugate is shown as an example.

Table 1
Physico-chemical characterization of PGA-fasudil conjugates.

Conjugate	Linker	Yield, %	Conj. eff., %	TDL, % wt[a]	FD, % wt[b]	R_h, nm[c]
PGA-F	Amide	87	92	13.7	0.01	4.8
PGA-O-F	Carbamate	65	87	12.4	0.1	4.9
PGA-SS-F	Self-immolative disulfide	84	85	11.5	0.1	5.1

[a] Determined by UV–Vis.
[b] Determined by HPLC (UV–Vis) and calculated as % of total drug loading.
[C]Hydrodynamic radius measured via DLS instrument in PBS expressed as mean volume. TDL – Total drug release.

to the distinct linkers. The protease-sensitive linker of PGA-F and the pH-sensitive linker of PGA-O-F failed to release significant levels of fasudil under appropriate conditions, with only 1.5% release in the presence of cathepsin B (PGA-F) (Figure SI5) and 12 % after five days at pH 7.4 (PGA-O-F) observed (Figure SI5). We observed more encouraging results for the redox responsive linker employed in PGA-SS-F when evaluating fasudil release in the presence of 5 mM and 10 μM DTT, which we employed to mimic the intracellular and extracellular concentrations of glutathione, respectively. In the presence of 5 mM DTT, we observed rapid drug release with zero-order kinetics during the first 6 h, reaching 80 % of total drug release after 8 h and approximately 100 % after 24 h. In the presence of 10 μM DTT, we failed to observe any drug release, even after 72 h (Fig. 2A). Figure SI6 details the mechanism of fasudil release from the PGA-SS-F conjugate under reductive environment, the intermediates, and the corresponding MS and MS/MS spectra.

To finalize the characterization of the PGA-SS-F conjugate and explore therapeutic potential, we studied stability in plasma and cell medium (Fig. 2B and C, Table 2, and Figure SI7) by LC-MS/MS, which provides insight into the fate of PGA-SS-F conjugate after administration. We calculated the concentration of free fasudil in plasma (Fig. 2B) and cell medium (Fig. 2C), sampled at defined time points and presented the values as a percentage of the free drug compared to the total concentration of conjugated fasudil. The percentage of free drug increased to only 3.15% (Figs. 2B) and 3.21 % (Fig. 2C) of total drug release over the 24 h in plasma and cell medium stability studies, respectively, thereby highlighting the high extracellular stability of the *PGA-SS-F* conjugate afforded by the disulfide linking moiety in agreement with the release studies (Fig. 2A). Conjugates from linear polymers, including those using PGA as a carrier, typically exhibit a blood $t_{1/2}$ lower than 24 h and accumulate rapidly within the lesion site after administration [12,20,23]; therefore, a 3 % loss of total drug loading will not significantly impact therapeutic performance. The LC-MS method employed has been fully validated for the determination of fasudil concentration in plasma, evaluating within-run and between-run accuracy, within-run, and between-run precision, matrix effects, and recovery values (Table 2).

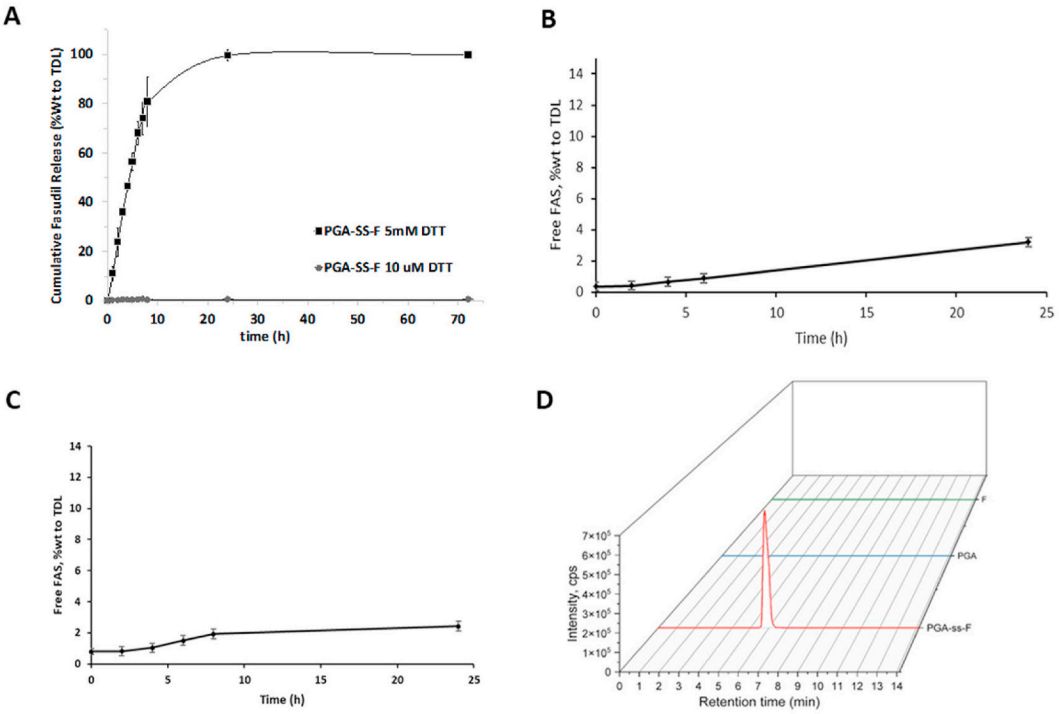

Fig. 2. Evaluation of Fasudil Release Kinetics and PGA-SS-F Conjugate Stability in Physiologically Relevant Media: A. Fasudil release from PGA-SS-F under redox conditions (5 mM [black squares] and 10 μM [grey circles] DTT). Data presented mean ± SEM (n = 3); B. Plasma stability study for the PGA-SS-F conjugate. Values presented as free fasudil % wt to total drug loading. Data presented as mean ± SEM (n = 3). C. Cell medium stability study for the PGA-SS-F conjugate. Values presented as free fasudil % wt to total drug loading. Data presented as mean ± SEM (n = 3). D. LC-MS/MS chromatograms of CSF samples analyzed 24h after the injection of PGA-SS-F and controls (PGA and F).

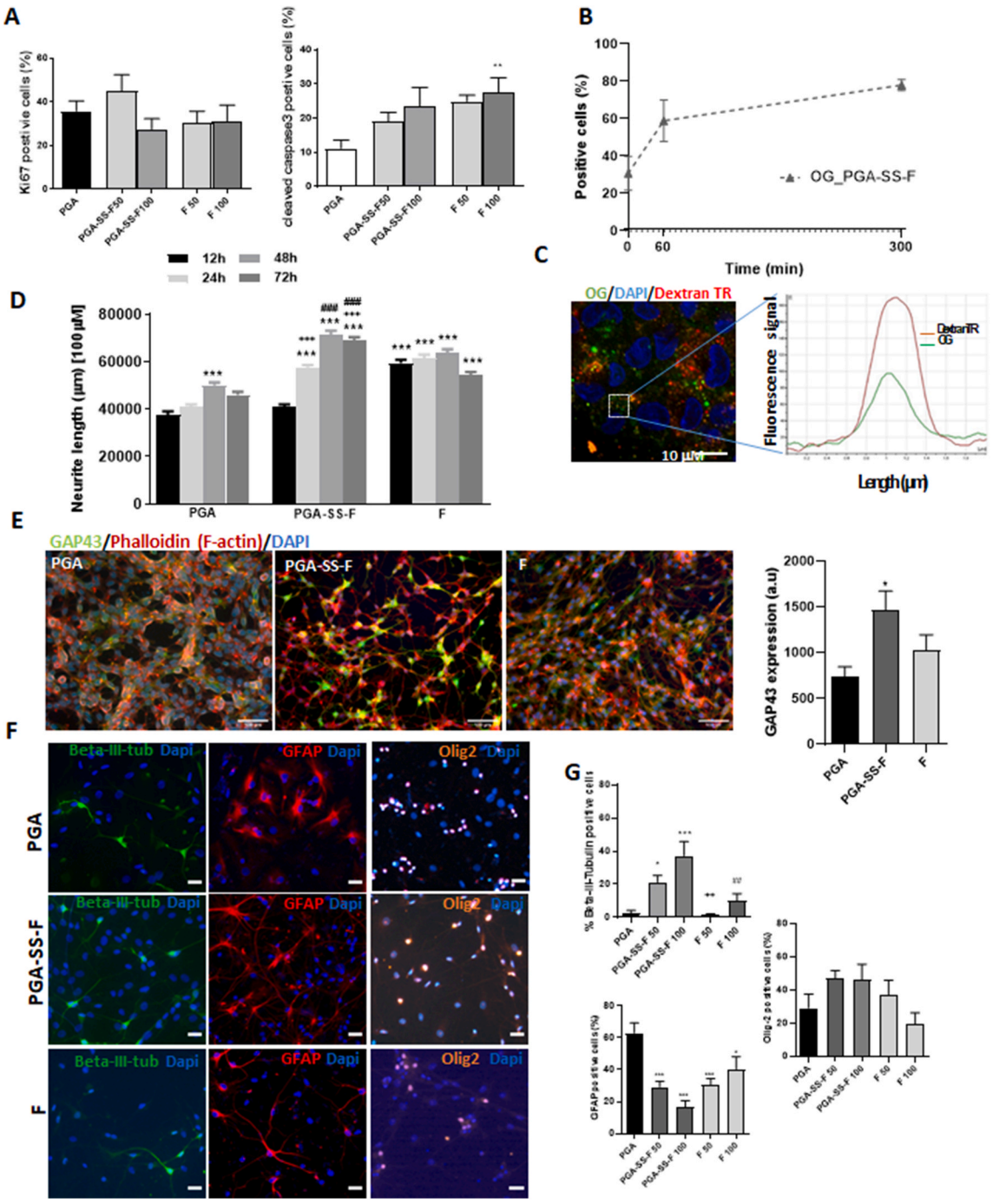

Fig. 3. *In vitro* Effects of PGA-SS-Fasudil Conjugate on NPC Survival, Differentiation, and Neurite Outgrowth. A. Quantification of NPCs positive for Ki67 (left panel) and cleaved caspase 3 (right panel) normalized to the total number of cells (DAPI positive, blue) treated for 24 h with 50 or 100 μM of PGA-SS-F or fasudil or the equivalent of PGA. Data expressed as mean ± S.E.M (n = 3 of independent experiments per group). **p < 0.01 vs. PGA, determined by ANOVA multiple comparison test and Tukey's *post hoc* test. B, C. Oregon green (OG) labeled conjugate (PGA-SS-F-OG) internalized into neurospheres-like cultures via an endocytic energy-dependent mechanism. B) Quantification of positive cells after confocal images acquisition at 0-, 60-, and 300-min incubation time. C) Representative confocal image at 300 min incubation time of PGA-SS-F demonstrates the internalization of the OG-linked compound and the co-localization in the lysosomes labeled with Dextran-TR (red). Data presented as mean ± SEM (n = 3). D. Quantification of neurite length of Matrigel-adhered NPCs following exposure to PGA (control) or 50 μM of free fasudil (F) or PGA-SS-F (at 50 μM, fasudil equiv.) for 12, 24, 48, or 72 h. Data presented as mean ± SEM (n = 3 of independent experiments per group) ***p < 0.001 vs. PGA 12h; +++p < 0.001 PGA-SS-F vs. fasudil 48h; ###p < 0.001 PGA-SS-F vs. fasudil 72 h determined by ANOVA multiple comparison test and Tukey's *post hoc* test. E. Representative images of immunofluorescent double-staining of GAP43 (green) and phalloidin (red) in NPCs treated as indicated (left panels); Quantification of GAP43 immunofluorescent staining (graph). F. Representative images of immunofluorescent staining of beta-III-tubulin (green), GFAP (red), and Olig-2 (orange) in NPCs treated as indicated. G. Quantification of immunofluorescent staining. Data presented as mean ± SEM (n = 3 of independent experiments per group) ^p < 0.05 *vs.* PGA determined by Kruskal-Wallis multiple comparison test *p < 0.05, **p < 0.05, ***p < 0.001 vs. PGA; $^{++}$p<0.01 vs. PGA-SS-F 50 μM; $^{\#\#}$p < 0.01 vs. PGA-SS-F 100 μM, determined by ANOVA multiple comparison test and Tukey's *post hoc* test. Scale bar: 20 μm. (For interpretation of the references to colour in this figure legend, the reader is referred to the Web version of this article.)

Table 2
LC-MS/MS method validation for the determination of fasudil concentration in plasma, evaluating within-run and between-run accuracy, within-run and between-run precision, matrix effects, and recovery values.

	Within-run		Between-run		Matrix effects		Recovery	
Sample	Accuracy (%)[a]	Precision (RSD_{pooled} %)	Accuracy (%)[a]	Precision (RSD_{pooled}%)	MF_{fas}/MF_{ran}	RSD (%)	R, %	RSD, %
LLOQ	−11.49	10.68	−10.10	9.52	0.96	2.83	76.51	3.23
Medium QC	−3.01	5.21	−3.01	5.83	0.99	2.01	78.90	5.14
LLOQ	−2.89	3.18	−2.88	3.15	1.01	1.81	81.34	1.47

[a] The difference from nominal value; RSD_{pooled} – pooled relative standard deviation; MF – matrix factor; RSD – relative standard deviation, n = 3; R – recovery.

3.2. PGA-SS-F improves neurogenesis and neuronal differentiation without influencing NPC survival

To evaluate the tolerability of the PGA-SS-F conjugate and the other conjugated forms (PGA-F and PGA-O-F) in rat NPCs, we evaluated cell viability at 50 μM (non-toxic dose for free fasudil) or 100 μM (toxic dose for free fasudil) equiv. concentrations for 24 h. While fasudil induced a significant decrease in NPC viability at 100 μM, the family of PGA-fasudil conjugates failed to induce any significant toxicity at the concentrations tested (Figure SI8A).

We next explored the effect of PGA-SS-F treatment on NPC proliferation and apoptosis by immunostaining for Ki67 in neurosphere-like cultures and cleaved caspase 3 in adherent conditions (Matrigel-coated substrate), respectively, at 50 and 100 μM in comparison with PGA or free fasudil (Fig. 3A). While we failed to encounter significant differences in proliferation in any of the conditions, we did observe a significant increase in apoptosis for 100 μM fasudil compared to PGA treatment, a finding that agrees with the findings of the cell viability assays (Figure SI8A). We employed an additional control condition (NPCs without PGA treatment (control)); however, we did not observe any significant differences in comparison with PGA-treated NPCs in the percentage of Ki67 positive cells (33.1 ± 2.7 for control vs. 35.9 ± 4.6 for PGA) or the percentage of caspase3 positive cells (9.1 ± 1.1 for control vs. 11.2 ± 2.4 for PGA).

Cell internalization studies suggested that the PGA-SS-F conjugate followed an energy-dependent endocytic mechanism with rapid intracellular accumulation (measured by quantifying the percentage of cells containing the Oregon green (OG)-labeled conjugate at 37 °C) (Fig. 3B and Figure SI8B). Confocal analysis provided evidence that most of the internalized conjugate moved into the lysosomal compartment (Dextran-TR employed as a lysosomal marker), indicating that fasudil release mainly occurs through a lysosomotropic mechanism [17] (Fig. 3C), in agreement with the release/stability data shown in Fig. 2. To ratify this finding and demonstrate that the presence of a reductive environment triggers fasudil release from PGA-SS-F, we studied the intracellular concentration of GSH in NPCs cells. We determined an intracellular concentration of GSH and GSSG of 7.42 ± 0.78 μM and 0.19 ± 0.03 μM, respectively, resulting in a GSH:GSSH ratio of 39:1 (experimental details in SI). In cells, the ratio of [GSH]/[GSSG] varies from 30:1 to 100:1, making the intracellular environment highly reducing; therefore, the presence of a disulfide bond is highly unlikely under these conditions. Reported data shows that a GSH:GSSG ration of ≥ 8:1 maintains protein disulfide isomerase (PDI) in a fully reduced state, suggesting the presence of only the reduced form of intracellular PDI [39].

We next discovered that NPC treatment with PGA-SS-F induced higher neurite elongation levels than free fasudil after 48 and 72 h of incubation in comparison with PGA-treated NPCs. We failed to encounter any significant differences when comparing PGA-treated NPCs to control (without PGA) (*data not shown*). Fasudil treatment significantly induced neurite outgrowth in NPCs as previously described [40,41]; however, this effect receded after 48 h of incubation. Interestingly, PGA-SS-F maintained neurite elongation for up to 72 h (Fig. 3D and Figure SI8C), thereby indicating a sustained long-term effect for fasudil conjugated through a self-immolative linker.

In agreement with the observed longer neurite processes, NPCs displayed significant morphological changes after 48 h of treatment with PGA-SS-F when compared with PGA- or free fasudil-treated NPCs, which exhibited a neuron-like shape (Fig. 3E). PGA-SS-F-treated NPCs exhibited a prominent soma with long and thin cellular projections stained with phalloidin; however, we observed few cell contacts in PGA-treated NPCs. Fasudil-treated NPCs also displayed a neuronal-like shape but with a less prominent soma and thicker projections than those observed for PGA-SS-F. Moreover, PGA-SS-F treatment induced a significant increase in the expression of growth-associated protein 43 (GAP43) in NPCs compared to PGA, free fasudil treatment (Fig. 3E, green), or control (without PGA; *data not shown*). GAP43 expression is classically related to neuronal axon growth and is associated with axon regeneration [42].

Previous studies demonstrated that fasudil promotes NPC differentiation and neurite outgrowth [43]; therefore, we evaluated whether exposure to PGA-SS-F could promotethe spontaneous neuronal differentiation of NPCs (Fig. 3F and G). We treated NPCs with PGA, fasudil, or PGA-SS-F at 50 or 100 μM fasudil equivalents and evaluated beta-III-tubulin, GFAP, and Olig2 expression levels as an indicator of differentiation into a neuronal, astrocytic, or oligodendrocytic fate, respectively (Fig. 3F and G). PGA-SS-F, but not fasudil, induced significant levels of beta-III-tubulin expression when compared to PGA treatment, with the 100 μM treatment affording a significantly higher increase than the 50 μM treatment, thereby indicating a possible dose-responsive effect on neuronal differentiation. Control conditions without PGA did not show significant differences when compared with PGA-treated NPCs (*data not shown*). Additionally, treatments with PGA-SS-F or fasudil prompted a highly significant decrease in GFAP expression, suggesting the inhibition of astrocyte differentiation. Finally, we failed to observe any significant alterations in Olig2 expression under any of the experimental conditions.

Overall, these findings suggest that PGA-SS-F treatment induces neuronal differentiation of NPCs at the expense of astrocytic differentiation - an effect that would benefit neuronal reorganization and local circuit re-activation after SCI upon transplantation of NPCs pre-treated with PGA-SS-F.

3.3. PGA-SS-F promotes greater axonal outgrowth in mature neurons from DRG explants

Neonatal rat DRG explants represent a suitable model for the study of axonal elongation, with high survival rates and robust responses to external stimuli. To measure the differential capacity of the various treatments to induce axon outgrowth, we exposed DRG neonatal explants to 50 μM fasudil-equiv. of free fasudil and PGA-SS-F or PGA (same polymer concentration as used in PGA-SS-F) for eight days and then co-stained with beta-III-tubulin, for further evaluation of neurite outgrowth extension and organization (Fig. 4A and B), and GAP43, whose expression indicates axonal growth (Fig. 4C) [42].

We determined the number of growing axons (beta-III-tubulin-positive) from the explant body and growth distance using NeuriteJ (Image J plug-in [34]) with the following values: i) Sholl critical value (RC), defined as the distance where the maximum number of dendrites intersect (indicating the branching degree), ii) the maximum number of

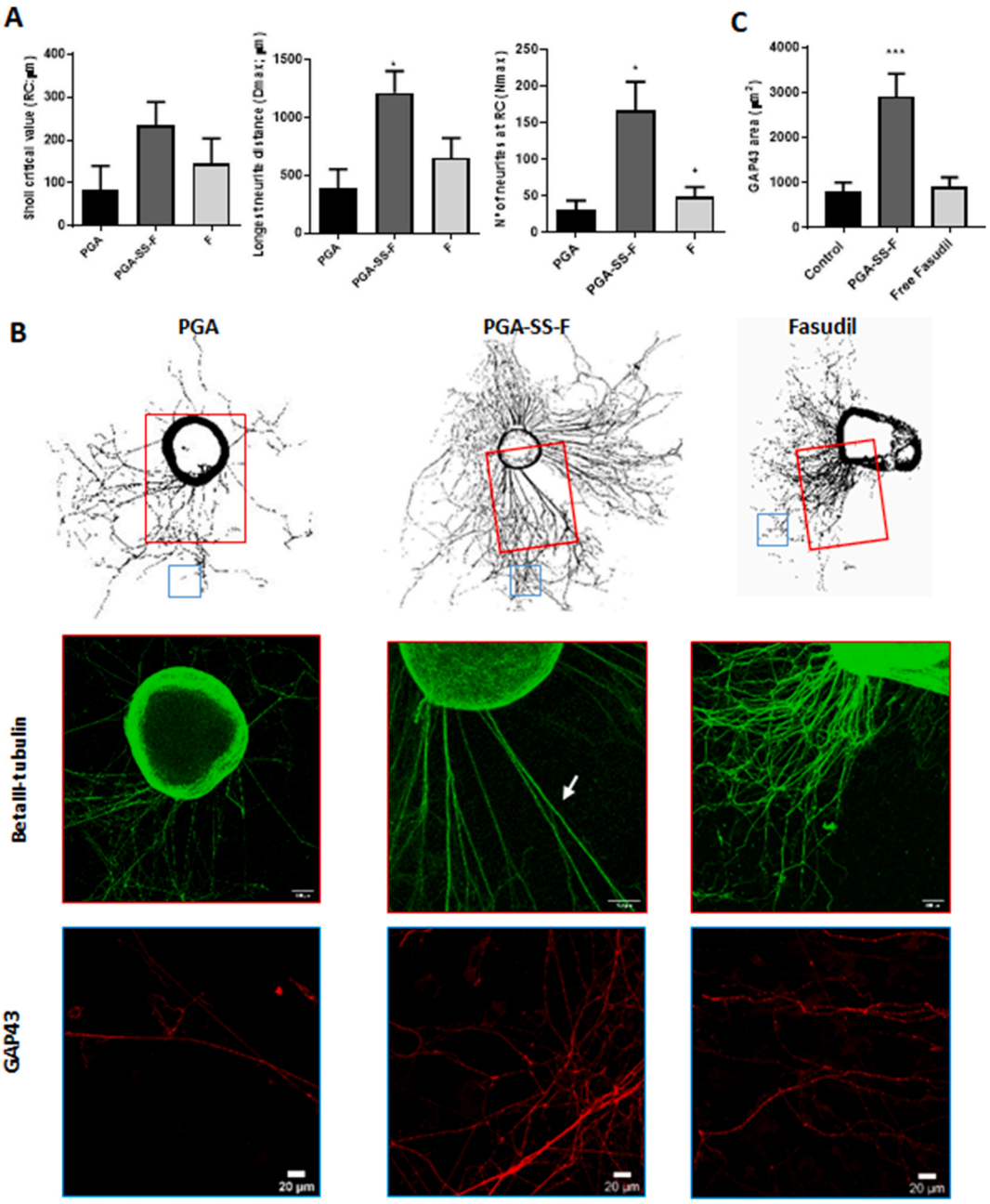

Fig. 4. PGA-SS-F Treatment Promotes Axonal Outgrowth in DRG Explants. A. Quantification of the maximal distance of axonal growth (D_{max}), the distance where the maximum number of axons intersect (Sholl critical value; RC), and the maximum number of axons intersecting at RC distance (N_{max}) in DRG explants using NeuriteJ plug-in. B. Upper panels: Representative image of a panoramic view for beta III-tubulin and GAP43 staining of those employed for axonal outgrowth quantification by NeuriteJ plug-in (quantifications shown in A from beta III-tubulin-stained images) and GAP43; lower panels: Immunofluorescence staining of beta-III-tubulin (green) from the selected area (red square in upper panels) and GAP43 from the selected area (blue square in upper panels) (red) and beta III-tubulin (green). C) Quantification of GAP43 occupied area. Data presented as mean ± SEM (n = 4 of independent experiments and a total of 6 DRGs per group were quantified) *$p < 0.05$, ***$p < 0.001$ vs. PGA and F groups determined by ANOVA multiple comparison test and Tukey's *post hoc* test. Scale bars, 100 μm for whole explants and 20 μm for individual images. (For interpretation of the references to colour in this figure legend, the reader is referred to the Web version of this article.)

neurites at the RC distance (N_{max}), and iii) the distance of the longest neurite (D_{max}). The combination of these three values serves to describe the different growth patterns [34]. As shown in Fig. 4A, we discovered that PGA-SS-F treatment increased the RC value compared to PGA and fasudil treatment although this failed to reach significance; however, we did observe a significant increase in the D^{max} and N^{max} values for PGA-SS-F, but not fasudil, compared to PGA treatment.

PGA-SS-F-treated DRG cultures stained with beta-III-tubulin also displayed significantly higher neurite outgrowth, as evidenced by measuring the total axon length projecting from the soma and the neuronal projections organized into thick and aligned bundles of fibers positive for beta III-tubulin when compared to PGA or fasudil treatment (as indicated in the PGA-SS-F image by a white arrow - Fig. 4B). In comparison, PGA or fasudil treatment prompted the outgrowth of thinner neuronal projections as randomly oriented processes (Fig. 4B).

PGA-SS-F treatment also prompted significant increases in the GAP43 occupied area compared with PGA and fasudil (Fig. 4B), in agreement with differentiating cultures of NPCs (Fig. 3F), indicating an active axon growth process that would contribute to the development of longer neurites in mature neurons. When compared with either PGA or

free fasudil, PGA-SS-F significantly induced the growth of neurons from DRG explants (Fig. 4A), increasing the maximum number of their neurites and generating the longest projections demonstrating the potential of our newly developed conjugate for axonal outgrowth and neuronal regeneration.

3.4. PGA-SS-F Preserves Neurofilaments and Increases Synaptophysin Expression and Axonal Outgrowth in an Ex Vivo Model of SCI in Organotypic Spinal Cord Slices

To evaluate the effects of PGA-SS-F in neuronal preservation and

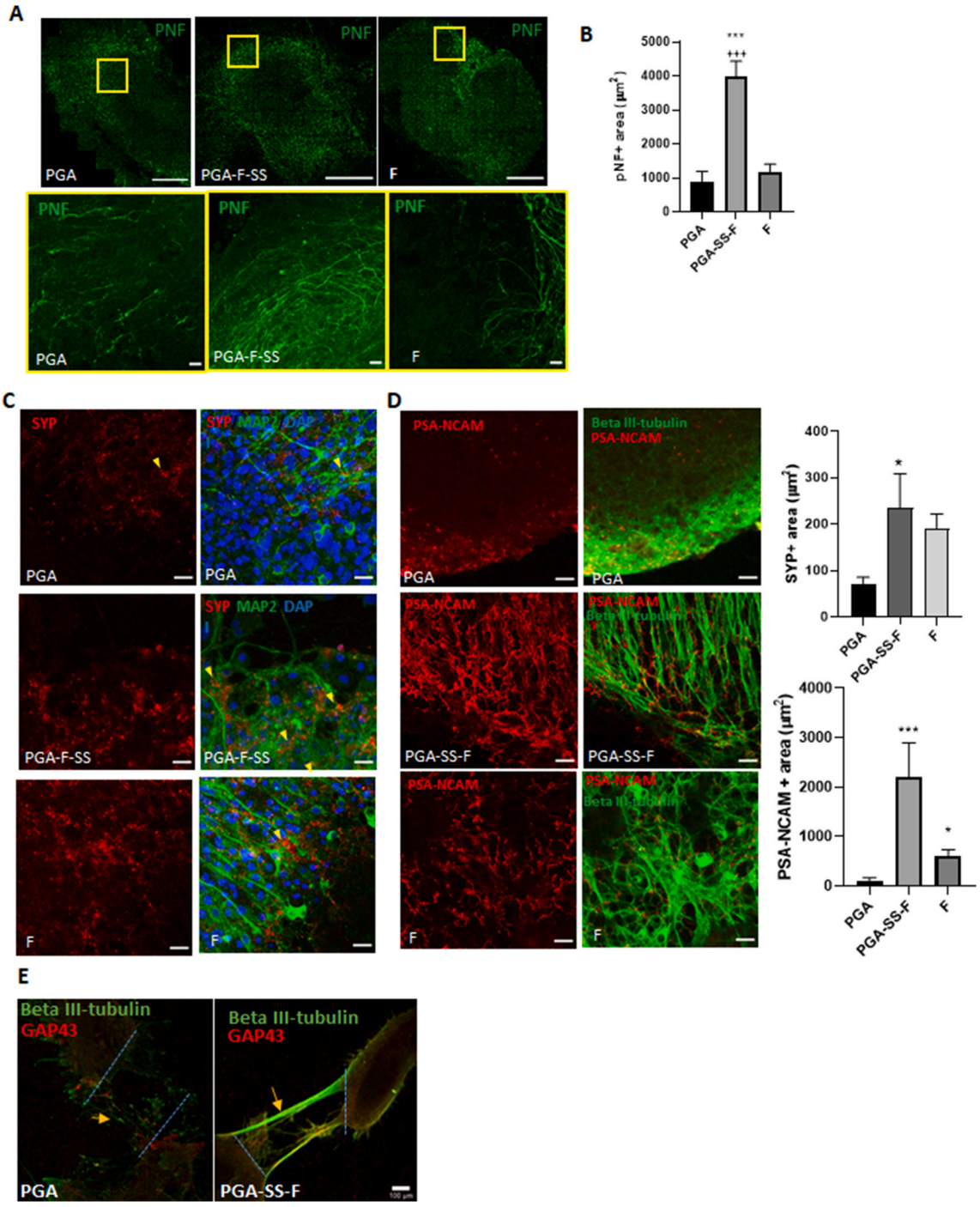

Fig. 5. PGA-SS-F Treatment Preserves a Greater Number of Neurofilaments and Induces Synaptic Features in Spinal Cord Organotypic *Ex Vivo* Cultures. A. Upper panels: Representative panoramic images of organotypic cultures of transversal slices of neonatal spinal cords. Scale bar 500 µm; Lower panels: Zoom images from yellow squares indicated in upper panels; scale 20 µm. B. Quantification of the area occupied by pNFs. C. Synaptophysin (SYP, red) and MAP-2 (green) stinaings; D. left panels: PSA-NCAM (red) and beta-III tubulin (green) in organotypic cultures treated with 50 µM of PGA-SS-F or fasudil or PGA (control) for one week. Scale bar 20 µm;. right panels: quantification of SYP vesicles and PSA-NCAM protein positive area. Data presented as mean ± SEM (n = 3 per group) *p < 0.05, ***p < 0.001 vs. PGA, $^{+}$p<0.05, $^{+++}$p<0.001 vs. F group and determined by ANOVA multiple comparison test and Tukey's *post hoc* test. E. Confocal image depicts an experiment with the greatest outgrowth and reconnections stained with beta-III-tubulin (green) and GAP43 (red) double immunostaining; n = 4. PGA-SS-F treated slices exhibited bundles of fibers crossing the lesion site, re-connecting both stumps (yellow arrows), positive for both beta-III-tubulin (green) and GAP43 (red). Blue dash lines delimited the lesion site. (For interpretation of the references to colour in this figure legend, the reader is referred to the Web version of this article.)

neuroplasticity in the spinal cord, we employed postnatal rat spinal cord organotypic cultures. We treated transversal spinal cord sections (350 μm) seven days after tissue section and damage with PGA, PGA-SS-F, and fasudil (at 50 μM drug equiv.) and then maintained cultures for five additional days. As the expression of phosphorylated neurofilaments (pNF) constitutes a key event in the regulation of axonal transport and provides stability to mature axons [44], both of relevance for axon regrowth, we evaluated pNF levels under different conditions. Representative images of pNF immunostaining (Fig. 5A) and the quantified data (Fig. 5C) demonstrate that PGA-SS-F treated slices exhibited significantly greater positive area for neuronal phospho-filaments than the PGA or fasudil, indicating that PGA-SS-F promotes active axonal transport on preserved fibers damaged by the sectioning process.

PGA-SS-F-treated injured spinal cord slices also allowed for the preservation of neuronal fibers, which displayed staining for microtubule-associated protein 2 (MAP2) (Fig. 5B; upper panels green). Furthermore, PGA-SS-F-treated injured spinal cord slices displayed significantly higher synaptic vesicle density in MAP2-positive neurons, as evidence by the increased synaptophysin (SYP) positive area (Fig. 5C, red) when compared to PGA or fasudil treatment. These findings suggest enhanced ex vivo synaptogenesis in response to PGA-SS-F-treatment.

The brain expresses high levels of polysialylated neuronal cell adhesion molecule (PSA-NCAM) during development, and expression in the adult is linked to functional plasticity [45]; therefore, increasing PSA-NCAM levels have been proposed as a therapeutic mechanism that may promote neuroregeneration following SCI [46]. We explored whether the PGA-SS-F treatment modulates PSA-NCAM expression in spinal cord slices. Representative images of PSA-NCAM immunostaining (Fig. 5D, lower panels; red) and the quantification of expression levels exhibited a significant increase in PSA-NCAM in beta-III tubulin positive neuronal fibers when compared to PGA or fasudil treatment (***$p < 0.001$ vs. PGA & fasudil) (Fig. 5D).

Following a transversally-induced lesion in longitudinal spinal cord slices that generates a gap between both stumps (Fig. 5E, dashed blue line), we evaluated the capacity of PGA-SS-F to re-connect the two sides of the lesion in comparison with PGA. We found that PGA-SS-F efficiently promoted axonal outgrowth in all assayed organocultures (Fig. 5E; the representative image shows the case with the longest reconnection). PGA-SS-F treated slices exhibiting bundles of beta-III-tubulin positive fibers (green) co-expressing GAP43 protein (red) that cross the lesion site and re-connect both stumps five days after lesion and treatment.

3.5. PGA-SS-F increases neurite regrowth following Rho/ROCK activation

Lysophosphatidic acid (LPA), a potent mitogen that activates the Rho/ROCK pathway, induces growth cone retraction and neurite collapse [47,48], and, therefore, mimics the molecular consequences of SCI in model systems. We studied the response of NPCs to LPA-induced Rho/ROCK pathway activation after treatment with PGA-SS-F or fasudil.

We first evaluated the capacity of PGA-SS-F to prevent neurite retraction induced by Rho/ROCK activation induced by LPA by Nestin immunostaining. LPA treatment reduced neurite length by nearly 50 % in NPCs when compared to PGA (Fig. 6A, yellow arrows); however, both PGA-SS-F and fasudil treatment significantly rescued LPA-induced neurite retraction (***$p < 0.001$ vs. LPA). (Fig. 6A, graph). Indeed, PGA-SS-F treatment of NPCs induced increased neurite length to a higher degree than PGA or fasudil treatment, even in the presence of LPA (Fig. 6A).

We also analyzed the effect of Rho/ROCK activation on the spontaneous differentiation of NPCs in the presence of PGA-SS-F. LPA treatment alone limited cell maturation and maintained a significant percentage of NPCs in an undifferentiated stage, as evaluated by the percentage of cells expressing Nestin (Fig. 6B, lower panel). We failed to find any differences in the number of Nestin-positive cells between control (without PGA) and PGA (46.77 ± 4.3 vs. 59.08 ± 2.14); however, PGA-SS-F in the presence of LPA led to significantly higher levels of beta-III-tubulin when compared to PGA or LPA alone, suggesting a preferential induction of a neuronal fate (Fig. 6B). Indeed, we failed to observe any significant differences in the glial markers Olig2 (early oligodendrocyte marker) and GFAP (astrocytic marker) under any of the studied conditions. As shown in Fig. 6C, we found that both free fasudil and PGA-SS-F efficiently inhibited LPA-induced phosphorylation of myosin phosphatase targeting protein (MYPT), a direct downstream target of Rho/ROCK in NPCs.

Finally, we performed a co-culture of eGFP-NPC (NPCs constitutively expressing eGFP) pre-treated with PGA, PGA-SS-F, or fasudil with the spinal cord organotypic cultures to mimic cell transplantation. PGA-SS-F-treated eGFP-NPCs (50 μM concentration for 24 h) displayed better engraftment when compared to non-pre-treated NPCs and displayed a neuronal-like morphology with an increased percentage of elongated cells (Fig. 6D, white arrow) when compared to NPCs pre-treated with PGA or fasudil, which mostly displayed a more rounded morphology (Fig. 6D, red arrow). We also discovered that PGA-SS-F-treated NPCs resided over long axonal/dendrite processes of the endogenous neurons of the spinal cord slices (Fig. 6D, red); in contrast, PGA- or fasudil-pretreated NPCs displayed lower cell density. This data indicates that NPCs pre-treated with PGA-SS-F exhibit enhanced engraftment abilities upon transplantation into the spinal cord.

3.6. In vivo administration of PGA-SS-F enhances neuroprotection and neuroregeneration related-signaling pathways in acute SCI

To investigate the capacity of PGA-SS-F to efficiently mitigate SCI-associated secondary injury at the acute stage after SCI in comparison with the free form of fasudil, we evaluated the consequences of a single local administration of PGA-SS-F or fasudil and PGA (10 μL/300 μM fasudil equiv. concentration) after severe experimental SCI. We evaluated protein levels of lysates from T7 to T9 spinal cord segments of at least four different animals, including the epicenter of the lesion induced at T8, 48 h after injury and treatment.

Sample analysis first revealed the significant inhibition of Rho kinase activity after PGA-SS-F treatment compared to PGA, as evidenced by the decreased phosphorylation of MYPT. Western blot images of four tested samples per each group (Fig. 7A) and the corresponding densitometry analysis (Fig. 7A, graph) demonstrate the efficacy of the local administration of the conjugate in reducing Rho kinase activity after SCI. We also collected CSF at the time of animal sacrifice and measured remaining fasudil levels within the intrathecal space via a validated LC-MS method (Fig. 2D and SI7). The LC-MS/MS conditions employed were identical to those used above to analyze fasudil stability in plasma. Nevertheless, we re-evaluated the developed LC-MS and extraction methods for linearity, LOQ, LOD, recovery, and matrix effects (Figure SI7). We found 1.29 % ± 0.08 % ($n = 3$) of total fasudil in the CSF collected 48 h after PGA-SS-F administration, although we failed to detected fasudil in CSF collected 48 h after injection of PGA or fasudil (Fig. 2D). These findings confirm the prolonged bioavailability of fasudil after PGA conjugation, supporting its greater pharmacological activity.

PGA-SS-F treatment significantly activated survival and anti-apoptotic molecular signaling, as evidenced by the significantly decreased the expression of caspase-3 in comparison with PGA or fasudil (Fig. 7B). In addition, PGA-SS-F treatment also significantly increased expression of the anti-apotic protein Bcl-2 and reduced the expression of the pro-apoptotic protein Bag1 in comparison with PGA treatment (Figure SI11A). This neuroprotective effect could be related to the observed significant increase in p-Akt levels (which can induce pro-survival related-signaling) in addition to the activation of autophagy, as revealed by a significant decrease in the phosphorylation of mTOR and significant increases to AMPK and LC3I levels following PGA-SS-F treatment (Figure SI11B).

Interestingly, PGA-SS-F treatment also displayed significant

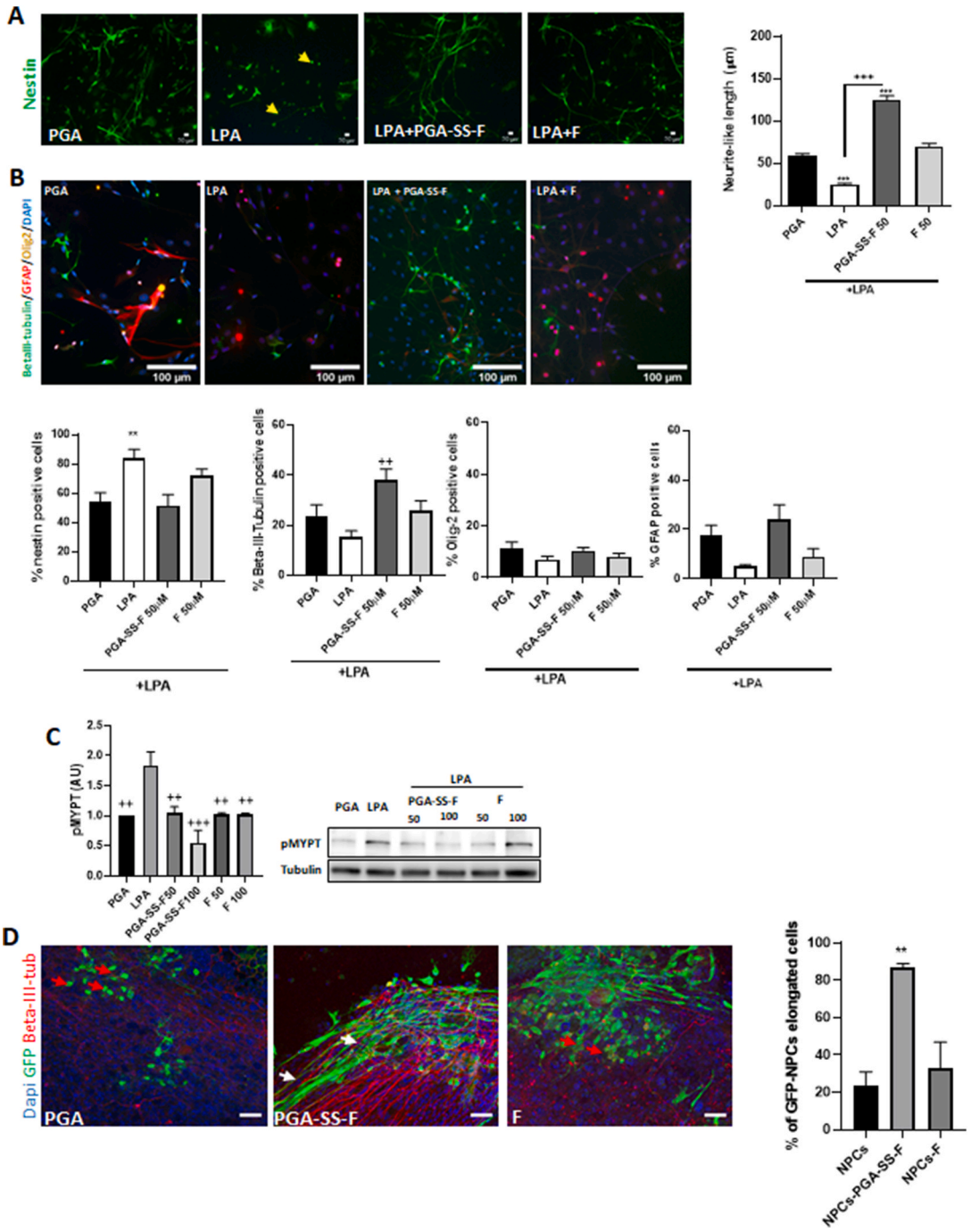

Fig. 6. PGA-SS-F Treatment Counters Neurite Retraction Following Rho/ROCK Activation and Promotes Neuronal Fate, Axonal Growth, and Neuroplasticity following Exposure to LPA in Spinal Cord Organotypic *Ex Vivo* Cultures. A. Left panels: NPCs treated with PGA (control) or fasudil/PGA-SS-F (50 μM) in adherent culture with representative immunostaining of Nestin (green). LPA treatment (10 μM) induced neurite retraction (yellow arrows); Right panel: Quantification of the longest neurite from each nestin-positive cell using NeuronJ. Data presented as mean ± SEM (n = 6 per group) ***$p < 0.001$ vs. PGA group; $^{+++}p<0.001$ vs. LPA group, determined by ANOVA multiple comparison test and Tukey's *post hoc* test. B. Upper panels: Representative images of beta-III-tubulin (green), Olig-2 (orange), and GFAP (red) immunostainings after spontaneous differentiation of NPCs treated as indicated. Lower panels: Quantification of the percentage of neurons (beta-III-tubulin positive), oligodendrocytes (Olig-2 positives), astrocytes (GFAP positive) and Nestin following ROCK activation in the presence of fasudil/PGA-SS-F (50 μM). Data presented as mean ± SEM (n = 3 per group) **$p < 0.01$ vs. PGA; $^{++}p<0.01$ vs. LPA determined by ANOVA multiple comparison test and Tukey's *post hoc* test. C. Quanitfication of phospho-MYPT levels by Western blotting in NPCs treated with LPA, fasudil, or PGA-SS-F. The relative expression of the protein bands was normalized to tubulin levels. Data presented as mean ± SEM (n = 3 per group) $^{++}p<0.01$ $^{+++}p<0.001$ vs. LPA determined by ANOVA multiple comparison test and Tukey's *post hoc* test. Representative blot is shown. D. Co-culture of PGA-SS-F or fasudil pre-treated eGFP-NPCs with organotypic neonatal spinal cord cultures. Left panels: Representative images of beta-III-tubulin (red) and GFP (green) immunostaining; Right panels: Quantification of elongated and engrafted NPCs, expressed as a percentage of total engrafted cells. PGA-SS-F pre-treated NPCs displayed increased neurite-like processes. Data presented as mean ± SEM (n = 3 per group). **$p <$ 0.01 vs. NPCs and NPCs–F groups determined by ANOVA multiple comparison test and Tukey's *post hoc* test. Scale bar 50 μm. (For interpretation of the references to colour in this figure legend, the reader is referred to the Web version of this article.)

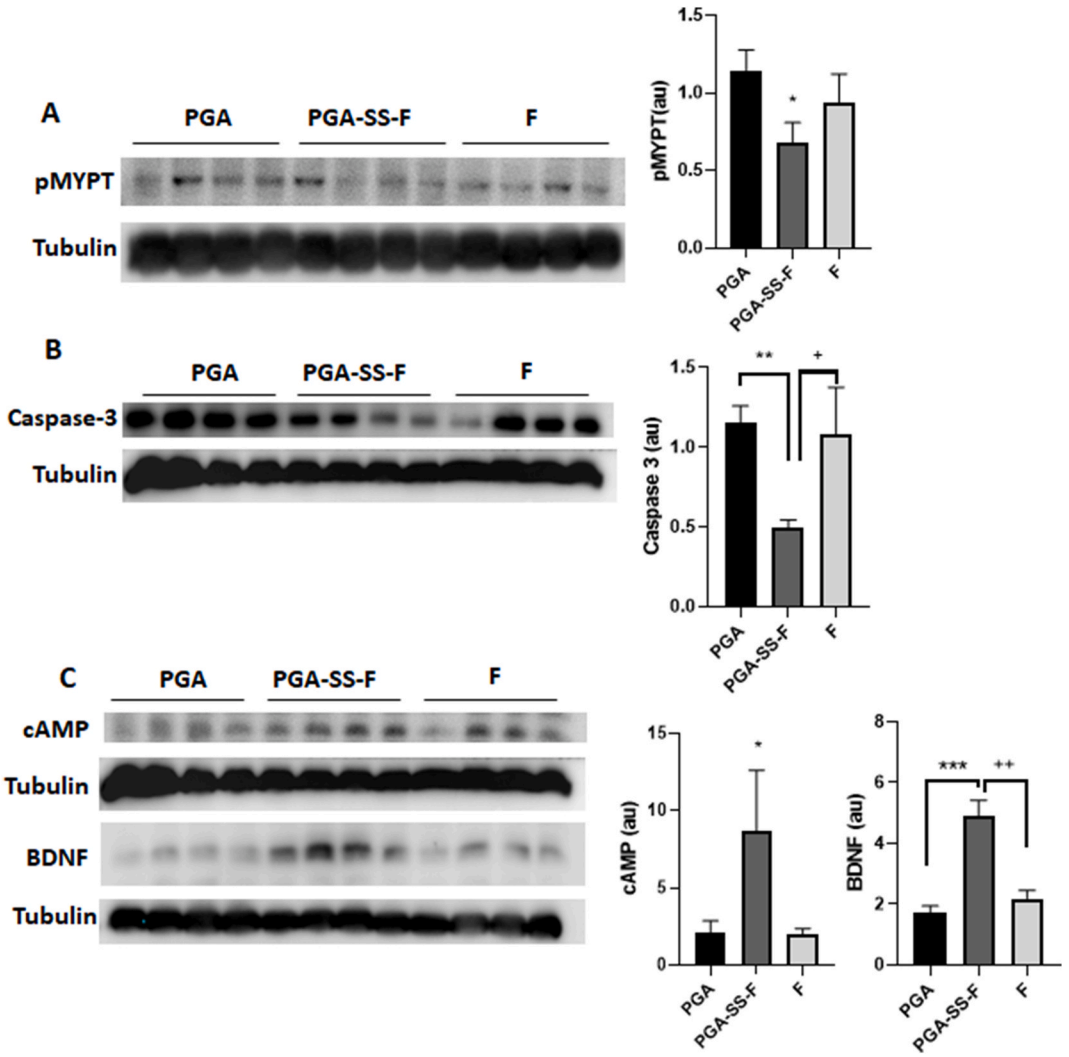

Fig. 7. Intrathecal Administration of PGA-SS-F but not the free form of fasudil Inhibits Rho/Rock Activity and Triggers Neuroprotective and Neuroregenerative Signaling Pathways 48 h after Acute SCI in vivo. A. Phospho-MYPT analysis as a proxy for Rho/Rock activation status following SCI. Graph represents the relative expression of the protein bands standardized by densitometry analysis to tubulin levels and presented as mean ± SEM (PGA and PGA-SS-F groups, n = 8; F group, n = 4). B. Analysis of the pro-apoptosis-related protein levels caspase-3. Graph represents the relative expression of the protein bands standardized by densitometry analysis to tubulin levels and presented as mean ± SEM. C. Analysis of pro-regenerative signaling via the evaluation of cAMP and pro-BDNF protein expression. Graph represents the relative expression of the protein bands standardized by densitometry analysis to tubulin levels and presented as mean ± SEM. *p < 0.05; **p < 0.01; **p < 0.001 vs. PGA group, $^{+}$p<0.05; $^{++}$p<0.01 vs. F; determined by ANOVA multiple comparison test and Tukey's *post hoc* test.

increases in cyclic (c)AMP and brain-derived neurotrophic factor (BDNF) levels in comparison with PGA or free fasudil treatment (Fig. 7C). BDNF acts as an autocrine factor that maintains neural survival and regulates late axon development, which itself requires the stable elevation of cAMP levels [49].

Together, these data indicates that the in vivo administration of PGA-SS-F, but not free fasudil, activates survival pathways and provides a priming signaling for neuronal regeneration following SCI.

3.7. PGA-SS-F treatment improves NPC transplantation engraftment, survival, and functional locomotor outcomes in a traumatic SCI Rat model

We previously demonstrated the beneficial effects of NPC therapy in acute [32,33] and chronic [12] traumatic SCI; however, low levels of survival and engraftment represent significant limitations associated with NPC transplantation.

We evaluated whether PGA-SS-F pre-treatment (50 μM drug equiv., 24 h) could improve the survival and engraftment of transplanted NPCs during in vivo cell transplantation immediately after severe SCI when compared to fasudil treatment or transplantation of untreated NPCs. We inspected transversal sections of the spinal cord to evaluate the distribution of eGFP-labeled NPCs two months after SCI and transplantation over 4.5 mm length, at the epicenter of the injury as shown in the graphical representation on Fig. 8A. PGA-SS-F-treated eGFP-NPC showed a more extensive distribution from rostral to caudal regions showing a greater area under the curve when compared to untreated eGFP-NPCs (Fig. 8A). The quantification of the total eGFP-NPCs at the epicenter of the injury revealed an increased number of engrafted cells for PGA-SS-F-treated NPCs and fasudil-treated NPCs, compared untreated NPCs. Nevertheless, PGA-SS-F-treated NPCs exhibited increased engraftment compared to fasudil-treated NPCs (Fig. 8B). Representative image of the transversal spinal cord section for GFP and ED-1 co-staining, for eGFP-NPC and macrophages identification respectively, showed that the engrafted eGFP-NPCs (green) co-existed in a non-phagocyte stage with infiltrated macrophages (red) (Fig. 8C). For eGFP-NPC quantification, we discarded ED-1-engulfed cells. We performed cell fate evaluation of the transplanted cells by beta-III tubulin and GFAP double staining; however, we failed to observe positive

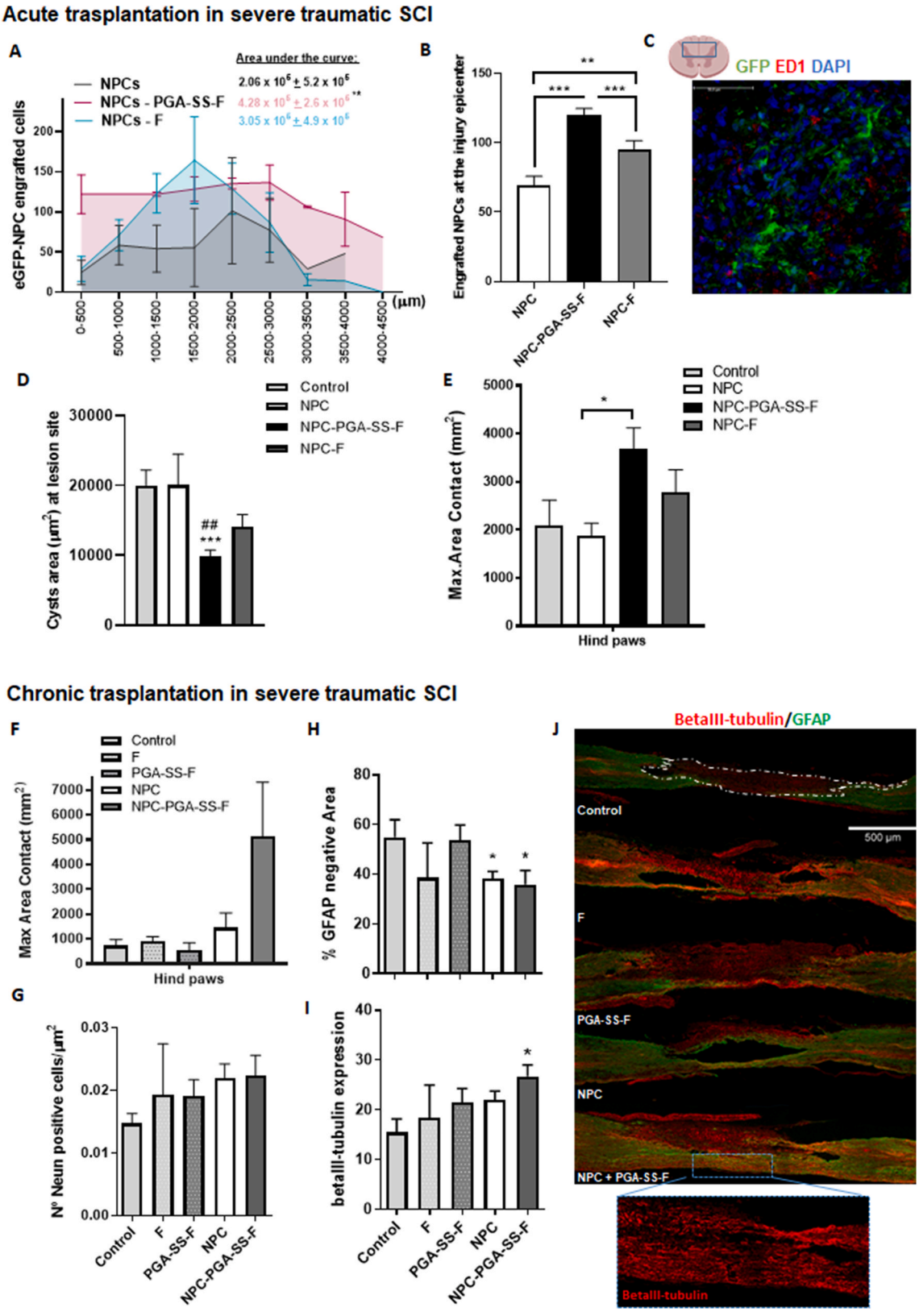

(caption on next page)

Fig. 8. *In vivo* Combination Treatment with PGA-SS-F improves NPCs Engraftment, Preserves Neuronal Fibers, and Promotes Gait Recovery. *Panels A-E correspond to the acute SCI model, while Panels F-J correspond to the chronic SCI model.* A. Analysis of engrafted eGFP-NPC distribution at the epicenter of the injury via the quantification of cells every 500 μm over 4.5 mm. The area under the curve obtained for each group over the 4.5 mm of the spinal cord is indicated in the corresponding legend. Data presented as mean ± SEM $^{**}p < 0.01$ vs. NPCs. B. Quantification of engrafted eGFP-NPCs at the epicenter of the injury. Data presented as mean ± SEM $^{**}p < 0.01$, $^{***}p < 0.001$ as indicated. C. Representative image of GFP (green) and ED1 (red) immunostaining showing non co-localization of transplanted eGFP-NPCs (positive for GFP) and infiltrated macrophages (positive for ED-1). D. Quantification of the cystic area by hematoxylin and eosin staining of spinal cord transversal sections eight weeks after SCI. Data presented as mean ± SEM. $^{***}p < 0.001$ compared to Conotrol and $^{\#\#}p < 0.01$ compared to NPC. E Gait analysis evaluation showing quantification of maximal area contact. Data presented as mean ± SEM. $^{*}p < 0.05$ compared as indicated. F. Gait analysis evaluation showing the maximal area contact of hind paws after treatments in the SCI chronic model. G. Quantification of NeuN positive cells per μm^2 H. Quantification of the GFAP negative area at the lesion site (area delimited in control group with a white dashed line in J). I. Quantification of beta-III-tubulin expression at the epicenter of the injury. J. Representative images of GFAP (green) and beta-III-tubulin (red) immunostainings in longitudinal spinal cord slices two months after treatments. Higher magnification of beta-III-tubulin fibers in NPCs + PGA-SS-F group shown in blue inset square. Data presented as mean ± SEM. $^{*}p < 0.05$ vs. control group. (For interpretation of the references to colour in this figure legend, the reader is referred to the Web version of this article.)

staining in transplanted eGFP-NPCs (*data not shown*).

We next employed hematoxylin and eosin staining of the spinal cord sections to evaluate cyst/cavity formation. PGA-SS-F-treated NPCs displayed smaller cavities compared to the control and NPC groups (Fig. 8D). Smaller cavities in the PGA-SS-F-treated NPC treated group could indicate tissue preservation, or the decrease in the cystic area could derive from the increased survival of transplanted cells, which, in turn, could fill the cavities.

Finally, in vivo functional analysis of gait by using CatWalk system two months after SCI and transplantation demonstrated improvement in certain locomotor skills measured by the increased maximum area of contact of the hind paws (Fig. 8E) in the group of animals transplanted with PGA-SS-F-treated NPCs. No other parameters analyzed in the CatWalk system showed significant differences (*data* not *shown*).

To evaluate the potential regenerative capacity of PGA-SS-F treatment alone or in combination with NPC transplantation in an extended neuronal degeneration process at the chronic spinal cord injury (five weeks after injury), we evaluated the simultaneous, but separate, application of both NPC transplantation and PGA-SS-F-treatment in chronic SCI. We hypothesized that the constant delivery of PGA-SS-F for one week into the intrathecal space using an osmotic pump would have an influence on both the transplanted eGFP-NPCs and the injured endogenous tissue. While the free form of fasudil demonstrated lower efficiency regarding NPC engraftment, survival, tissue preservation and functional improvement in the acute treatment (Fig. 8A–E), we did not test the combination with fasudil free form in the chronic injuries. None of the tested conditions prompted significant differences during CatWalk gain analysis, which measured the maximum contact area two months after the administration of fasudil or PGA-SS-F alone or after transplantation of NPC alone or in combination with PGA-SS-F (Fig. 8F). While the combination of PGA-SS-F and NPCs increased the maximum contact hind paws area, values failed to reach significance due to the generally high levels of variability in the measurement. The crossing time and stride length index also failed to indicate significant differences between the groups in any of the SCI models (*data* not *shown*).

We next inspected the spinal cord tissue two months after treatment. The quantification of mature neuronal somas using the NeuN marker at the injury site failed to reveal significant differences between groups (Fig. 8G); however, we did observe a significant reduction in the scar size (Fig. 8H), delimited by the astrocytic barrier, as measured as the percentage of GFAP negative area, following the transplantation of eGFP-NPCs alone or eGFP-NPCs combined with PGA-SS-F. Of note, a single administration of PGA-SS-F treatment failed to influence scar size (Fig. 8H).

Combined PGA-SS-F and eGFP-NPC transplantation prompted the appearance of a significantly higher amount of beta-III-tubulin positive fibers (Fig. 8I-J) within the injured tissue when compared with the PGA treatment as control, indicating a significant neuroprotective effect of the combination treatment in chronic stage SCI. Fig. 8J depicts representative immunostainings of beta-III-tubulin (red) for neuronal fiber detection (a higher magnification of beta-II-tubulin stainging is shown for the combinatory treatment from the indicated area; blue square) and GFAP (green) for astrocytic detection lining the astrocytic barrier (GFAP positive) and delimiting the formed scar (negative for GFAP; Fig. 8J, white dashed line), from one animal per group.

Overall, our data provide evidence that our redox-sensitive conjugated form of fasudil (PGA-SS-F) provides for enhanced NPC survival and integration, which prompted enhanced neuroprotection and repair within the injured SCI.

4. Discussion

Rho kinase signaling rapidly and dramatically activates following SCI [50–52] and contributes to secondary damage by triggering inflammation or apoptosis, among other mechanisms [53]. Rho kinase restrains neuronal polarization and axon growth by inducing myosin-II generated actin arcs to prevent microtubule protrusion in the axonal growth cone [54] and participates in axon tip collapse [4,53,55]. Genetic or pharmacological inhibition of RhoA/ROCK drives axonal regrowth and neuroprotection [50,56,57]; therefore, inhibition of RhoA/ROCK represents a candidate translational strategy to improve functional outcomes after SCI in humans. Several clinical trials of RhoA/ROCK inhibitors have been recently approved [5,58], with fasudil reaching evaluation in a phase III clinical trial, which provided evidence for utility and safety in acute ischemic stroke patients [59]. However, and importantly, the lower than anticipated efficacy of fasudil led to the termination of the trial, with the low stability in circulation and a general lack of penetration through the blood-brain barrier, presumably driving these poor results [8].

To address these limitations and potentiate the benefits of fasudil in SCI treatment, we developed a family of rationally designed polymer-fasudil conjugates based on PGA as a multivalent, biodegradable, and biocompatible carrier [14]. To achieve the site-specific and sustained release of fasudil after intrathecal administration, we explored polymer-drug linking strategies with relevance to the physiological conditions of the SCI lesion, which include the presence of proteases, pH gradients, and reducing environments. Therefore, we synthesized and fully characterized conjugates with a protease labile amide linker (PGA-F), a hydrolytically-labile carbamate linker (PGA-O-F), and a novel disulfide self-immolative (PGA-SS-F) linker susceptible to a reductive environment (Fig. 1) by post-polymerization modification approaches [19].

While we failed to observe toxicity in NPCs for any of the developed conjugates, free fasudil significantly reduced NPC viability at the highest tested concentration, suggesting that polymer conjugation will allow for an increase in the tolerated dose used in patients. Next, we evaluated the capacity of each conjugate to induce neurite elongation from NPCs under adherent conditions, as previously described for fasudil [43], in the hope of improving the integration and neuronal interconnection of NPCs into the damaged spinal cord neural network. Interestingly, PGA-SS-F exhibited a similar capacity to induce neuritogenesis over short periods as free fasudil, but more importantly, only PGA-SS-F prompted long-term neurite elongation (Fig. 3). These results could be explained by drug release kinetics, which demonstrated the higher

bioavailability of fasudil from the PGA-SS-F conjugate under intracellular reductive conditions (Figs. 2 and SI). This neuritogenic effect agrees with the preferential neuronal lineage commitment induced by PGA-SS-F in NPCs (Fig. 3).

Ex vivo experiments provided direct evidence that PGA-SS-F induced axonal outgrowth in both peripheral and central nervous system-derived neurons in neonatal DRG organotypic cultures (Fig. 4), adult dissociated DRGs (SI9), or spinal cord slices (Fig. 5) as evidenced by the induced axonal elongation and induced expression of GAP43, a known growth cone marker. Interestingly, the neuronal projections induced by the PGA-SS-F treatment were organized into thick bundles of aligned fibers with larger caliber axons and increased levels of synaptogenesis, as evidenced by the increased expression of synaptophysin in the spinal cord slice neuronal outgrowths. This marked effect on bundle formation could be derived from the increased number of pNFs found following PGA-SS-F treatment. Neurofilaments contribute to an increase in axonal diameter, while larger caliber axons possess more rapid conduction velocities than smaller axons [60]. Neurofilaments undergo phosphorylation to regulate transport and function, increase myelination, and induce stability during axonal growth in vivo [61]. Also, we discovered increased PSA-NCAM expression in the PGA-SS-F treated organotypic slices, indicating a fasciculation process, which contributes to the described bundle formation and, most probably the guiding process, thereby allowing the neuronal projections to re-connect within the spared tissue (Fig. 5F).

LPA treatment induces growth cone retraction and neurite collapse [47,48] in NPCs (Fig. 6). In conditions that mimic the over-activation of the RhoA/ROCK pathway that occurs in vivo after SCI, we demonstrated the enhanced capacity of PGA-SS-F to overcome LPA induced retraction and neural differentiation (Fig. 6) when compared with free fasudil, probably due to the higher Rho inhibitory activity of PGA-SS-F. In vivo, we discovered that a single intrathecal administration of PGA-SS-F immediately after SCI efficiently induced neuroprotection through the inhibition of RhoA/ROCK, a reduction in apoptosis, as evidence by detection of the activated form of caspase 3, and the induction of survival-related signaling factors, such as Bag-1, Bcl2 or, pAKT [62]. AKT phosphorylation could act as a focal point as the critical substrate of axon regeneration related pathways such as PI3K-PDK1, PI3K-mTORC2, mTORC1, or GSK3β [63]. Therefore, selective activation of the AKT pathway could provide for induced neuroprotection and neuroregeneration. Indeed, brief treatment with PGA-SS-F induced a significant accumulation of cAMP, an axonal growth mediator, and the neurotrophin BDNF but not the free fadudil form, indicating the activation of additional regenerative signals (Fig. 7). Increasing cAMP levels enhances the growth and guidance of axons, opposes the inhibitory signaling exerted by myelin and the glial scar [64], and increases the intrinsic capacity of injured axons to regrow [65] with the aid of BDNF [66]. Also, at early times after injury (48 h), PGA-SS-F significantly reduced the phosphorylation of mTOR (Figure SI11). Inhibition of mTOR phosphorylation during the acute phase of SCI can prevent neural cell death by limiting apoptosis [67,68] and reduce secondary damage mediated by microglial activation and migration [69]. Furthermore, the neuroprotective effects of inhibiting mTOR can be achieved by activating autophagy; rapamycin treatment (a specific inhibitor of mTOR) induces autophagy [70] and enhances lysosomal biosynthesis, thereby offering neuroprotection following central nervous system injury [71]. Decreased or blocked autophagic flux has been described in SCI [72], with downregulated autophagic activity related to increased neuronal apoptosis [73], which was more evident in ventral horn motor neurons than in sensory neurons [74]. We also found evidence for the modulation of autophagy by PGA-SS-F treatment by an increase in pAMPK and LC3 levels in vivo (Figure SI11), with LC3 and AMPK reported to contribute to autophagosome maturation and lysosomal fusion [75]. We further explored the potential implication of AMPK activation in neurite outgrowth induced by PGA-SS-F (Figure SI10). Pre-treatment with the AMPK phosphorylation inhibitor compound C (CC), significantly reduced neurite elongation from NPCs in culture; however, the inhibition of AMPK activation failed to abolish the neuritogenic effect of PGA-SS-F, thereby arguing against the involvement of the activation of this pathway (Figure SI10).

Poor engraftment, low survival, and astrocytic differentiation represent the significant reported limitations of stem cell-based therapies for SCI [76,77]. As PGA-SS-F promotes the survival of NPCs offering a great advantage for cell transplantation, we primed NPCs with PGA-SS-F before transplantation in the hope of overcoming the hostile microenvironment associated with acute-phase SCI. Results revealed that NPCs primed with PGA-SS-F treatment displayed enhanced survival after acute transplantation, with significant higher engraftment extending rostral and caudally to the lesion, significantly greater when compared with the transplanted NPC primed with the free form of fasudil, accompanied by reduced cavitation and increased locomotor skills recovery, as measured as the maximum paw contact area during stepping (Fig. 8A–E). Transplanted cells failed to contribute to astrogliosis; moreover, transplanted NPC failed to show preferential differentiation into a neuronal cell fate since no co-localization with either GFAP or beta-III-tubulin, respectively. These findings indicate that the dedifferentiation of NPCs into an immature stage occurs independently of the PGA-SS-F treatment. We previously reported that spinal cord-derived NPCs transplanted after SCI express Olig2 [31], a marker of undifferentiated oligodendrocytes, indicating a preferential oligodendroglia rather than neuronal or astroglial cell fate.

In the chronic SCI scenario, we previously reported that spinal cord-derived NPCs in combination with a polymer-curcumin conjugate prompted a significant improvement in functional locomotor recovery after transplantation. While conjugate treatment failed to induce any significant effect when administered alone, the combination with NPCs led to improvements above and beyond those observed with the transplantation of NPCs alone [12]. We employed a similar approach by combining PGA-SS-F and NPC transplantation in severe chronic SCI by direct administration into the injured area (Fig. 8F–J). The combination of treatments, PGA-SS-F delivered within an osmotic pump for a week, and the NPCs, intramedullary injected rostral and caudal to the lesion, prompted a more significant amount of beta III-tubulin fibers at the lesion site two months after treatment, as previously shown for the combination of the polymer-curcumin conjugate and NPC [12]. Furthermore, a significant number of these fibers possessing a straightened, organized pattern indicating an anatomical guided preservation suggesting protection of the ultrastructural organization of the long tracts. Although gait performance analysis showed non-significant differences among the groups and variability between the samples, the combination treatment group displayed a better gait response in the SCI chronic model.

5. Conclusion

Herein, we report on the transplantation of spinal cord-derived NPCs in combination with a polymer conjugated form of the Rho kinase inhibitor fasudil for the treatment of SCI. We improved the therapeutic potential of fasudil, with a short serum half-life, through conjugation to a polypeptidic carrier via an optimized redox-dependent self-immolative linker. PGA conjugation enhanced stability, sustained fasudil release, and improved neuroprotective and regenerative activity in acute and chronic in vivo models of SCI. Furthermore, PGA-SS-F treatment of transplanted NPCs improved tissue engraftment and cell survival, and so, this may represent an important approach towards the development of successful cell transplantation strategies.

Declaration of competing interest

The authors declare the following financial interests/personal relationships which may be considered as potential competing interests: Patent application filed for PGA-SS-F conjugate (PCT/EP2020/058940)

co-inventors EG, VJN, OZ, RRA, AA, AA, SD, MJV, and VMR. No other commercial conflicts of interest are present.

Acknowledgments

This research was funded by FEDER/Ministerio de Ciencia e Innovación – Agencia Estatal de Investigación [RTI2018-095872-B-C21/ERDF], Ministerio de Ciencia e Innovación [SAF2016-80427-R, PID2019-108806RB-I00], Fundació Marató TV3 [20172230, 20172231 and 20172110] Fundación Step by Step, Agencia Valenciana de Innovación (AVI) [INNVAL10/19/047] and MINECO/FEDER, UE; Fondo Europeo de Desarrollo Regional (FEDER) incluido en el Programa Operativo FEDER de la Comunidad Valenciana 2014–2020.

Appendix A. Supplementary data

Supplementary data to this article can be found online at https://doi.org/10.1016/j.biomaterials.2021.121052.

Authors contribution

E. Giraldo: Conceptualization; Data curation; Formal analysis; Investigation; Methodology; Roles/Writing – original draft; Writing – review & editing. V.J. Nebot: Conceptualization; Data curation; Formal analysis; Investigation; Methodology. S Đorđević: Data curation; Formal analysis; Investigation; Methodology; Writing – review & editing. Raquel Requejo-Aguilar: Conceptualization; Data curation; Formal analysis; Investigation; Methodology. A. Alastrue-Agudo: Investigation; Methodology. O. Zagorodko: Data curation; Formal analysis; Investigation; Methodology; Writing – review & editing. A. Armiñan: Data curation; Formal analysis; Investigation; Methodology; B. Martinez-Rojas: Investigation; Methodology. M.J. Vicent: Conceptualization; Data curation; Formal analysis; Roles/Writing – original draft; Writing – review & editing; Funding acquisition; Project administration. Moreno-Manzano: Conceptualization; Data curation; Formal analysis; Roles/Writing – original draft; Writing – review & editing; Funding acquisition; Project administration.

Data availability

The data that support the findings of this study are available on request from the corresponding author. The data are not publicly available due to privacy or ethical restrictions.

References

[1] C.S. Ahuja, M. Fehlings, Concise review: bridging the gap: novel neuroregenerative and neuroprotective strategies in spinal cord injury, Stem cells translational medicine 5 (2016) 914–924.
[2] E.J. Bradbury, E.R. Burnside, Moving beyond the glial scar for spinal cord repair, Nat. Commun. 10 (2019) 3879.
[3] T. Madura, T. Yamashita, T. Kubo, M. Fujitani, K. Hosokawa, M. Tohyama, Activation of Rho in the injured axons following spinal cord injury, EMBO Rep. 5 (2004) 412–417.
[4] Y. Fujita, T. Yamashita, Axon growth inhibition by RhoA/ROCK in the central nervous system, Front. Neurosci. 8 (2014) 338.
[5] R. Watzlawick, E.S. Sena, U. Dirnagl, B. Brommer, M.A. Kopp, M.R. Macleod, et al., Effect and reporting bias of RhoA/ROCK-blockade intervention on locomotor recovery after spinal cord injury: a systematic review and meta-analysis, JAMA Neurol 71 (2014) 91–99.
[6] D. Impellizzeri, E. Mazzon, I. Paterniti, E. Esposito, S. Cuzzocrea, Effect of fasudil, a selective inhibitor of Rho kinase activity, in the secondary injury associated with the experimental model of spinal cord trauma, J. Pharmacol. Exp. Therapeut. 343 (2012) 21–33.
[7] S. Hasegawa, Y. Hasegawa, M. Miura, Current therapeutic drugs against cerebral vasospasm after subarachnoid hemorrhage: a comprehensive review of basic and clinical studies, Curr. Drug Deliv. 14 (2017) 843–852.
[8] B.K. Mueller, H. Mack, N. Teusch, Rho kinase, a promising drug target for neurological disorders, Nat. Rev. Drug Discov. 4 (2005) 387–398.
[9] V. Gupta, N. Gupta, I.H. Shaik, R. Mehvar, I.F. McMurtry, M. Oka, et al., Liposomal fasudil, a rho-kinase inhibitor, for prolonged pulmonary preferential vasodilation in pulmonary arterial hypertension, J. Contr. Release 167 (2013) 189–199.
[10] I. Ekladious, Y.L. Colson, M.W. Grinstaff, Polymer-drug conjugate therapeutics: advances, insights and prospects, Nat. Rev. Drug Discov. 18 (2019) 273–294.
[11] K. Maso, A. Grigoletto, M.J. Vicent, G. Pasut, Molecular platforms for targeted drug delivery, Int Rev Cell Mol Biol. 346 (2019) 1–50.
[12] R. Requejo-Aguilar, A. Alastrue Agudo, M. Cases Villar, E. Lopez-Mocholi, R. England, M.J. Vicent, et al., Combined polymer-curcumin conjugate and ependymal progenitor/stem cell treatment enhances spinal cord injury functional recovery, Biomaterials 113 (2017) 18–30.
[13] O. Zagorodko, J.J. Arroyo-Crespo, V.J. Nebot, M.J. Vicent, Polypeptide-Based Conjugates as Therapeutics: Opportunities and Challenges. Macromol Biosci (2017) 17.
[14] A. Duro-Castano, I. Conejos-Sánchez, M.J. Vicent, Peptide-based polymer therapeutics, Polymers 6 (2014) 515–551.
[15] A. Varela-Moreira, Y. Shi, M.H.A.M. Fens, T. Lammers, W.E. Hennin, R. M. Schiffelers, Clinical application of polymeric micelles for the treatment of cancer, Materials Chemistry Frontiers 1 (2017) 16.
[16] R. Duncan, Polymer therapeutics at a crossroads? Finding the path for improved translation in the twenty-first century, J. Drug Target. 25 (2017) 759–780.
[17] J.J. Arroyo-Crespo, C. Deladriere, V.J. Nebot, D. Charbonnier, E. Masiá, A. Paul, et al., Anticancer activity driven by drug linker modification in a polyglutamic acid-based combination-drug conjugate, Adv. Funct. Mater. 28 (2018) 18.
[18] A. Duro-Castano, N.H. Lim, I. Tranchant, M. Amoura, F. Beau, H. Wieland, et al., Vivo imaging of MMP-13 activity using a specific polymer-FRET peptide conjugate detects early osteoarthritis and inhibitor efficacy, Adv. Funct. Mater. (2018) 28.
[19] M. Barz, A. Duro-Castano, M.J. Vicent, A versatile post-polymerization modification method for polyglutamic acid: synthesis of orthogonal reactive polyglutamates and their use in "click chemistry, Polym. Chem. 4 (2013) 2989–2994.
[20] J.J. Arroyo-Crespo, A. Arminan, D. Charbonnier, L. Balzano-Nogueira, F. Huertas-Lopez, C. Marti, et al., Tumor microenvironment-targeted poly-L-glutamic acid-based combination conjugate for enhanced triple negative breast cancer treatment, Biomaterials 186 (2018) 8–21.
[21] N.L. Trevaskis, L.M. Kaminskas, C.J. Porter, From sewer to saviour - targeting the lymphatic system to promote drug exposure and activity, Nat. Rev. Drug Discov. 14 (2015) 781–803.
[22] A. Duro-Castano, V.J. Nebot, A. Nino-Pariente, A. Arminan, J.J. Arroyo-Crespo, A. Paul, et al., Capturing "extraordinary" soft-assembled charge-like polypeptides as a strategy for nanocarrier design, Adv. Mater. (2017) 29.
[23] A. Duro-Castano, R.M. England, D. Razola, E. Romero, M. Oteo-Vives, M. A. Morcillo, et al., Well-defined star-shaped polyglutamates with improved pharmacokinetic profiles as excellent candidates for biomedical applications, Mol. Pharm. 12 (2015) 3639–3649.
[24] I. Conejos-Sánchez, A. Duro-Castano, A. Birke, M. Barz, M.J. Vicent, A controlled and versatile NCA polymerization method for the synthesis of polypeptides, Polym. Chem. 4 (2013) 3182–3186.
[25] E.S. Rosenzweig, J.H. Brock, P. Lu, H. Kumamaru, E.A. Salegio, K. Kadoya, et al., Restorative effects of human neural stem cell grafts on the primate spinal cord, Nat. Med. 24 (2018) 484–490.
[26] E. Curtis, J.R. Martin, B. Gabel, N. Sidhu, T.K. Rzesiewicz, R. Mandeville, et al., A first-in-human, phase I study of neural stem cell transplantation for chronic spinal cord injury, Cell Stem Cell. 22 (2018) 941–950, e6.
[27] H. Kumamaru, K. Kadoya, A.F. Adler, Y. Takashima, L. Graham, G. Coppola, et al., Generation and post-injury integration of human spinal cord neural stem cells, Nat. Methods 15 (2018) 723–731.
[28] P. Assinck, G.J. Duncan, B.J. Hilton, J.R. Plemel, W. Tetzlaff, Cell transplantation therapy for spinal cord injury, Nat. Neurosci. 20 (2017) 637–647.
[29] H. Kumamaru, P. Lu, E.S. Rosenzweig, K. Kadoya, M.H. Tuszynski, Regenerating corticospinal axons innervate phenotypically appropriate neurons within neural stem cell grafts, Cell Rep. 26 (2019) 2329–2339, e4.
[30] F. Barnabe-Heider, C. Goritz, H. Sabelstrom, H. Takebayashi, F.W. Pfrieger, K. Meletis, et al., Origin of new glial cells in intact and injured adult spinal cord, Cell Stem Cell. 7 (2010) 470–482.
[31] V. Moreno-Manzano, F.J. Rodriguez-Jimenez, M. Garcia-Rosello, S. Lainez, S. Erceg, M.T. Calvo, et al., Activated spinal cord ependymal stem cells rescue neurological function, Stem Cell. 27 (2009) 733–743.
[32] A. Alastrue-Agudo, F.J. Rodriguez-Jimenez, E.L. Mocholi, F. De Giorgio, S. Erceg, V. Moreno-Manzano, FM19G11 and ependymal progenitor/stem cell combinatory treatment enhances neuronal preservation and oligodendrogenesis after severe spinal cord injury, Int. J. Mol. Sci. (2018) 19.
[33] R. Gomez-Villafuertes, F.J. Rodriguez-Jimenez, A. Alastrue-Agudo, M. Stojkovic, M.T. Miras-Portugal, V. Moreno-Manzano, Purinergic receptors in spinal cord-derived ependymal stem/progenitor cells and their potential role in cell-based therapy for spinal cord injury, Cell Transplant. 24 (2015) 1493–1509.
[34] A. Torres-Espín, D. Santos, F. González-Pérez, J. del Valle, X. Navarro, Neurite-J: an image-J plug-in for axonal growth analysis in organotypic cultures, J. Neurosci. Methods 236 (2014) 26–39.
[35] B. Bonnici, J.P. Kapfhammer, Spontaneous regeneration of intrinsic spinal cord axons in a novel spinal cord slice culture model, Eur. J. Neurosci. 27 (2008) 2483–2492.
[36] A. Alastrue-Agudo, S. Erceg, M. Cases Villar, V. Bisbal-Velasco, R.J. Griffeth, F. J. Rodriguez Jimenez, et al., Experimental cell transplantation for traumatic spinal cord injury regeneration: intramedullar or intrathecal administration, Methods Mol. Biol. 1210 (2014) 23–35.
[37] F. Hamers, A. Lankhorst, T. Van Laar, W. Veldhuis, W. Gispen, Automated quantitative gait analysis during overground locomotion in the rat: its application

to spinal cord contusion and transection injuries, J. Neurotrauma 18 (2001) 187–201.
[38] L.B. Vong, Y. Ibayashi, Y. Lee, D.N. Ngo, Y. Nishikawa, Y. Nagasaki, Poly (ornithine)-based self-assembling drug for recovery of hyperammonemia and damage in acute liver injury, J. Contr. Release 310 (2019) 74–81.
[39] A. Raturi, B. Mutus, Characterization of redox state and reductase activity of protein disulfide isomerase under different redox environments using a sensitive fluorescent assay, Free Radic. Biol. Med. 43 (2007) 62–70.
[40] S. Chen, M. Luo, Y. Zhao, Y. Zhang, M. He, W. Cai, et al., Fasudil stimulates neurite outgrowth and promotes differentiation in C17.2 neural stem cells by modulating notch signalling but not autophagy, Cell. Physiol. Biochem. 36 (2015) 531–541.
[41] Z.A. Nizamudeen, L. Chakrabarti, V. Sottile, Exposure to the ROCK inhibitor fasudil promotes gliogenesis of neural stem cells in vitro, Stem Cell Res. 28 (2018) 75–86.
[42] S.K. Doster, A.M. Lozano, A.J. Aguayo, M.B. Willard, Expression of the growth-associated protein GAP-43 in adult rat retinal ganglion cells following axon injury, Neuron 6 (1991) 635–647.
[43] S. Chen, M. Luo, Y. Zhao, Y. Zhang, M. He, W. Cai, et al., Fasudil stimulates neurite outgrowth and promotes differentiation in C17.2 neural stem cells by modulating notch signalling but not autophagy, Cell. Physiol. Biochem. 36 (2015) 531–541.
[44] T.B. Shea, C. Jung, H.C. Pant, Does neurofilament phosphorylation regulate axonal transport? Trends Neurosci. 26 (2003) 397–400.
[45] J.Z. Kiss, D. Muller, Contribution of the neural cell adhesion molecule to neuronal and synaptic plasticity, Rev. Neurosci. 12 (2001) 297–310.
[46] A. El Maarouf, A.K. Petridis, U. Rutishauser, Use of polysialic acid in repair of the central nervous system, Proc. Natl. Acad. Sci. U.S.A. 103 (2006) 16989–16994.
[47] K. Jalink, E.J. van Corven, T. Hengeveld, N. Morii, S. Narumiya, W.H. Moolenaar, Inhibition of lysophosphatidate- and thrombin-induced neurite retraction and neuronal cell rounding by ADP ribosylation of the small GTP-binding protein Rho, J. Cell Biol. 126 (1994) 801–810.
[48] O. Kranenburg, M. Poland, F.P. van Horck, D. Drechsel, A. Hall, W.H. Moolenaar, Activation of RhoA by lysophosphatidic acid and Galpha12/13 subunits in neuronal cells: induction of neurite retraction, Mol. Biol. Cell 10 (1999) 1851–1857.
[49] P.L. Cheng, A.H. Song, Y.H. Wong, S. Wang, X. Zhang, M.M. Poo, Self-amplifying autocrine actions of BDNF in axon development, Proc. Natl. Acad. Sci. U. S. A. 108 (2011) 18430–18435.
[50] C.I. Dubreuil, M.J. Winton, L. McKerracher, Rho activation patterns after spinal cord injury and the role of activated Rho in apoptosis in the central nervous system, J. Cell Biol. 162 (2003) 233–243.
[51] M.K. Erschbamer, C.P. Hofstetter, L. Olson, RhoA, RhoB, RhoC, Rac1, Cdc42, and Tc10 mRNA levels in spinal cord, sensory ganglia, and corticospinal tract neurons and long-lasting specific changes following spinal cord injury, J. Comp. Neurol. 484 (2005) 224–233.
[52] W.J. Wei, Z.Y. Yu, H.J. Yang, M.J. Xie, W. Wang, X. Luo, Cellular expression profile of RhoA in rats with spinal cord injury, J Huazhong Univ Sci Technolog Med Sci. 34 (2014) 657–662.
[53] X. Wu, X.M. Xu, RhoA/Rho kinase in spinal cord injury, Neural Regen Res. 11 (2016) 23–27.
[54] S. Dupraz, B.J. Hilton, A. Husch, T.E. Santos, C.H. Coles, S. Stern, et al., RhoA controls axon extension independent of specification in the developing brain, Curr. Biol. 29 (2019) 3874–3886, e9.
[55] J.C. Koch, L. Tatenhorst, A.E. Roser, K.A. Saal, L. Tönges, P. Lingor, ROCK inhibition in models of neurodegeneration and its potential for clinical translation, Pharmacol. Ther. 189 (2018) 1–21.
[56] P. Dergham, B. Ellezam, C. Essagian, H. Avedissian, W.D. Lubell, L. McKerracher, Rho signaling pathway targeted to promote spinal cord repair, J. Neurosci. 22 (2002) 6570–6577.
[57] F. Boato, S. Hendrix, S.C. Huelsenbeck, F. Hofmann, G. Grosse, S. Djalali, et al., C3 peptide enhances recovery from spinal cord injury by improved regenerative growth of descending fiber tracts, J. Cell Sci. 123 (2010) 1652–1662.
[58] M.G. Fehlings, K.D. Kim, B. Aarabi, M. Rizzo, L.M. Bond, L. McKerracher, et al., Rho inhibitor VX-210 in acute traumatic subaxial cervical spinal cord injury: design of the SPinal cord injury rho INhibition InvestiGation (SPRING) clinical trial, J. Neurotrauma 35 (2018) 1049–1056.
[59] M. Shibuya, S. Hirai, M. Seto, S. Satoh, E. Ohtomo, Fasudil Ischemic Stroke Study G. Effects of fasudil in acute ischemic stroke: results of a prospective placebo-controlled double-blind trial, J. Neurol. Sci. 238 (2005) 31–39.
[60] R.L. Friede, T. Samorajski, Axon caliber related to neurofilaments and microtubules in sciatic nerve fibers of rats and mice, Anat. Rec. 167 (1970) 379–387.
[61] R. Starr, B. Attema, G.H. DeVries, M.J. Monteiro, Neurofilament phosphorylation is modulated by myelination, J. Neurosci. Res. 44 (1996) 328–337.
[62] M.S. Song, L. Salmena, P.P. Pandolfi, The functions and regulation of the PTEN tumour suppressor, Nat. Rev. Mol. Cell Biol. 13 (2012) 283–296.
[63] L. Miao, L. Yang, H. Huang, F. Liang, C. Ling, Y. Hu, mTORC1 is necessary but mTORC2 and GSK3beta are inhibitory for AKT3-induced axon regeneration in the central nervous system, Elife 5 (2016) e14908.
[64] C. Aglah, T. Gordon, Posse de Chaves EI. cAMP promotes neurite outgrowth and extension through protein kinase A but independently of Erk activation in cultured rat motoneurons, Neuropharmacology 55 (2008) 8–17.
[65] S. Neumann, F. Bradke, M. Tessier-Lavigne, A.I. Basbaum, Regeneration of sensory axons within the injured spinal cord induced by intraganglionic cAMP elevation, Neuron 34 (2002) 885–893.
[66] Y. Ji, P.T. Pang, L. Feng, B. Lu, Cyclic AMP controls BDNF-induced TrkB phosphorylation and dendritic spine formation in mature hippocampal neurons, Nat. Neurosci. 8 (2005) 164–172.
[67] Z. Wang, L. Zhou, X. Zheng, G. Chen, R. Pan, J. Li, et al., Autophagy protects against PI3K/Akt/mTOR-mediated apoptosis of spinal cord neurons after mechanical injury, Neurosci. Lett. 656 (2017) 158–164.
[68] P. Tang, H. Hou, L. Zhang, X. Lan, Z. Mao, D. Liu, et al., Autophagy reduces neuronal damage and promotes locomotor recovery via inhibition of apoptosis after spinal cord injury in rats, Mol. Neurobiol. 49 (2014) 276–287.
[69] L. Xie, F. Sun, J. Wang, X. Mao, L. Xie, S.H. Yang, et al., mTOR signaling inhibition modulates macrophage/microglia-mediated neuroinflammation and secondary injury via regulatory T cells after focal ischemia, J. Immunol. 192 (2014) 6009–6019.
[70] X. Lin, L. Han, J. Weng, K. Wang, T. Chen, Rapamycin inhibits proliferation and induces autophagy in human neuroblastoma cells, Biosci. Rep. (2018) 38.
[71] S. Peña-Llopis, S. Vega-Rubin-de-Celis, J.C. Schwartz, N.C. Wolff, T.A. Tran, L. Zou, et al., Regulation of TFEB and V-ATPases by mTORC1, EMBO J. 30 (2011) 3242–3258.
[72] M.M. Lipinski, J. Wu, A.I. Faden, C. Sarkar, Function and mechanisms of autophagy in brain and spinal cord trauma, Antioxidants Redox Signal. 23 (2015) 565–577.
[73] S. Liu, C. Sarkar, M. Dinizo, A.I. Faden, E.Y. Koh, M.M. Lipinski, et al., Disrupted autophagy after spinal cord injury is associated with ER stress and neuronal cell death, Cell Death Dis. 6 (2015) e1582.
[74] T. Muñoz-Galdeano, D. Reigada, Velez I. Del Águila Á, M.J. Caballero-López, R. M. Maza, et al., Cell specific changes of autophagy in a mouse model of contusive spinal cord injury, Front. Cell. Neurosci. 12 (2018) 164.
[75] M. Jang, R. Park, H. Kim, S. Namkoong, D. Jo, Y.H. Huh, et al., AMPK contributes to autophagosome maturation and lysosomal fusion, Sci. Rep. 8 (2018) 12637.
[76] P. Lu, L. Graham, Y. Wang, D. Wu, M. Tuszynski, Promotion of survival and differentiation of neural stem cells with fibrin and growth factor cocktails after severe spinal cord injury, J. Vis. Exp. 89 (2014), e50641, https://doi.org/10.3791/50641.
[77] Y. Li, W.M. Zhang, T.H. Wang, Optimal location and time for neural stem cell transplantation into transected rat spinal cord, Cell. Mol. Neurobiol. 31 (2011) 407–414.